

Small- x physics in deep-inelastic lepton-hadron scattering

B. Badełek

Institute of Experimental Physics, Warsaw University, Warsaw, Poland

K. Charchuła*

Deutsches Elektronen-Synchrotron, DESY, Hamburg, Germany

M. Krawczyk

Institute of Theoretical Physics, Warsaw University, Warsaw, Poland

J. Kwieciński

Department of Theoretical Physics, H. Niewodniczanski Institute of Nuclear Physics, Cracow, Poland

This article reviews the physics of deep-inelastic lepton-hadron processes in the region of small x , where x is the Bjorken scaling variable. The theoretical concepts concerning the Regge limit of deep-inelastic scattering are summarized and recent theoretical results on the small- x limit of parton distributions in perturbative QCD are discussed. Presently available experimental data on the free- and bound-nucleon structure functions at small x are reviewed in detail and their theoretical interpretations (including the low- x , low- Q^2 region) are discussed. QCD predictions are given for the deep-inelastic scattering structure functions F_2 and F_L in the small- x ($10^{-5} < x < 10^{-2}$) and moderately large- Q^2 region relevant for HERA ($Q^2 \sim 10 \text{ GeV}^2$).

CONTENTS

| | |
|----------------------------------------------------------------------------------------|-----|
| I. Introduction | 927 |
| II. Theoretical Ideas | 928 |
| A. Definitions | 928 |
| B. Regge theory | 930 |
| C. Pomeron at high energies | 930 |
| D. Small x in deep-inelastic scattering on a nucleon | 931 |
| 1. Regge behavior of the structure functions in the parton model | 931 |
| 2. Evolution equations | 932 |
| 3. Screening corrections | 934 |
| 4. Types of parton parametrizations | 934 |
| E. Deep-inelastic diffraction | 937 |
| F. Low- x nuclear physics | 937 |
| G. Low- x , low- Q^2 phenomena | 939 |
| III. Experiments in the Low- x Region | 941 |
| A. List of experiments | 941 |
| 1. Muon (electron) scattering experiments | 941 |
| 2. Neutrino scattering experiments | 942 |
| B. Extraction of the structure functions, radiative corrections, and systematic errors | 942 |
| C. Results of the low- x structure-function measurements | 944 |
| 1. $R(x, Q^2)$ | 944 |
| 2. Nucleon structure functions from hydrogen and deuterium | 945 |
| 3. Nucleon structure function from heavy nuclei | 948 |
| 4. Structure-function ratios | 949 |
| a. $F_2(D)/F_2(H)$ | 949 |
| b. $F_2(A)/F_2(D)$ | 951 |
| IV. Probing the Small- x Region at HERA | 953 |
| V. Summary and Outlook | 956 |
| Acknowledgments | 957 |
| References | 957 |

I. INTRODUCTION

Deep-inelastic lepton-hadron scattering is a very powerful tool for studying the underlying parton (i.e., the quark and antiquark and, indirectly, also the gluon) structure of a nucleon. This process is described in terms of the structure functions, which are directly related to the quark and antiquark distribution functions in a nucleon.

The interaction of quarks and gluons is described by quantum chromodynamics (QCD). Deep-inelastic lepton scattering is a unique tool for testing QCD in its perturbative regime (Reya, 1981; Altarelli, 1982). The study of deep-inelastic lepton-nucleon scattering in the region of small x , where x is the Bjorken scaling variable, is very interesting both phenomenologically and theoretically. Among other things, it opens the way to the study and testing of QCD in a new kinematical regime where several new phenomena are expected to occur.

According to QCD, at low values of x ($x \sim 10^{-4}$) and at large values of Q^2 a nucleon consists predominantly of gluons and sea quarks. Their densities grow rapidly in the limit $x \rightarrow 0$, leading to possible spatial overlap and to interactions between the partons. Several novel physical phenomena are thus expected when parton densities are high, for example, shadowing or semihard processes appearing with large cross sections in the high-energy hadronic reactions (Gribov *et al.*, 1983; Levin and Ryskin, 1990a; Levin, 1991).

Over the past decade our knowledge of the nucleon structure functions, or the parton distributions in the nucleon, has greatly improved. A vast amount of data has been accumulated from neutral and charged-lepton scattering experiments at high values of the scattering variable, $x \geq 0.03$ (see, for example, Milsztajn *et al.*,

*On leave of absence from the Institute of Experimental Physics, Warsaw University.

1991). Below this limit the experimental data are still scarce, and a firm understanding and well established theoretical approach are still lacking.

The analysis of deep-inelastic scattering data from fixed-target experiments is now almost finished. It is thus important to summarize our knowledge of low- x phenomena and define goals to be set for the forthcoming experiments at the ep HERA collider, which is now being commissioned and which will allow us to probe the low- x region.

The presently running accelerators do not, in principle, permit the exploration of low- x physics at sufficiently large Q^2 values. For example, the CERN SPS permits nucleon structure-function measurements down to $x=0.006-0.008$ at $Q^2=3 \text{ GeV}^2$ with a high-energy muon beam. In contrast, the SLAC electron machine cannot achieve values of x smaller than 0.1. Measurements at the lowest values of x have been performed at both CERN and FNAL ($x > 0.002$ and $x > 0.00002$, respectively) at the expense of lowering the Q^2 value down to $0.1-0.01 \text{ GeV}^2$. The Tevatron, especially in its first stage, can offer slightly better possibilities, but the very best opportunities for measurements in the low- x region will be found at HERA, down to $x \sim 10^{-5}$, and at the LHC, down to $x \sim 10^{-6}$, at moderate values of Q^2 , as summarized in Fig. 1 (Tung *et al.*, 1989).

Several deep-inelastic scattering experiments have been performed on nuclear targets, and various nuclear effects have shown up at small x , as for example shadowing, which depletes the bound-nucleon structure function relative to that measured from free nucleons.

Small- x physics is a very complicated subject with scarce data and a variety of different theoretical approaches. There exist comprehensive theoretical reviews (Gribov *et al.*, 1983; Levin and Ryskin, 1990a; Levin, 1991) addressing the rather advanced reader. The data, on the other hand, are distributed over many publications. This paper provides a review of theoretical and ex-

perimental low- x ($x < 0.03$ or so) physics. Its aim is to introduce the *inexperienced* reader to this rich and fascinating field. We shall concentrate almost exclusively on lepton-hadron scattering, since most of the experimental and theoretical work is in this area. The paper consists of three parts:

A theoretical introduction, in which we present the important definitions and concepts relevant to the small- x region, i.e., elements of Regge theory, predictions of perturbative QCD for the small- x behavior of parton distributions, deep-inelastic diffraction, small- x nuclear physics, and specific problems of the low- Q^2 region (Sec. II);

A survey of the small- x experimental situation, including a description of methods for extracting the results from the measurements and a review of the low- x data (Sec. III);

A short presentation of theoretical predictions for the HERA small- x region (Sec. III).

The theoretical introduction has a form resembling a lexicon, where certain problems are only mentioned but always with relevant references (mainly to review articles). Wherever possible simple intuitive pictures are also given. The experimental problems and results are discussed in greater detail, since the lack of an established approach to small- x phenomena means that guidance from the data is important. The present paper provides the first collection of experimental results. We hope that this kind of presentation of low- x physics will be useful, especially for experimentalists and for those just beginning their work in this field. From this point of view our review is similar to the reports of Charchuła *et al.* (1990) and Abramowicz *et al.* (1991b), in which other topics related to ep scattering at HERA were discussed. The notation used here will be the same as in those papers.

II. THEORETICAL IDEAS

We shall start by discussing the elements of Regge theory and its consequences for deep-inelastic scattering on a nucleon. Then we consider evolution equations, screening corrections for structure functions, and deep-inelastic diffraction. Phenomena that appear at small x in the nuclear medium are discussed next. Finally, as the present small- x measurements were usually made at $Q^2 \leq 1 \text{ GeV}^2$, we found it necessary to summarize current knowledge of the low- Q^2 phenomena for both nucleon and nuclear targets.

A. Definitions

The small- x region of deep-inelastic scattering offers the unique possibility of exploring the Regge limit of perturbative QCD (Cheng and Wu, 1969; Frolov *et al.*, 1970; Landshoff and Polkinghorne, 1972; Collins, 1977; Balitskij and Lipatov, 1978; Bronzan and Sugar, 1978; Bartels, 1979, 1980; White, 1979; Jaroszewicz, 1980,

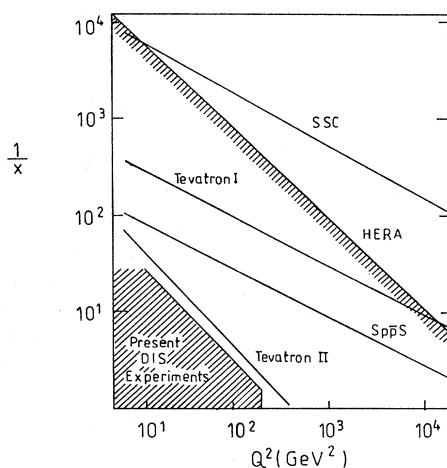


FIG. 1. Road map of high-energy physics in the 1990s (from Tung *et al.*, 1989).

1982; Lipatov and Szymanowski, 1980; Gribov *et al.*, 1983; Lipatov, 1989, 1976; Levin and Ryskin, 1990a, 1990b; Levin, 1991). To clarify this statement let us consider the deep-inelastic lepton-nucleon scattering (see also Charchuła *et al.*, 1990)

$$lN \rightarrow l'X, \tag{1}$$

where l' is the scattered lepton and X stands for the final hadronic state. The cross section for this process can be illustrated as in the left side of Fig. 2. The wavy line in the figure denotes the exchanged vector boson: γ or Z^0 for neutral current and W^\pm for charged-current interactions. At fixed energy the kinematics of inelastic lepton-nucleon scattering is determined by two independent variables. Let q and p be the momenta of the exchanged gauge boson and of the nucleon. The Bjorken scaling variable x is then defined as

$$x = Q^2/2p \cdot q = Q^2/2M\nu, \tag{2}$$

where M denotes the nucleon and where $-Q^2 = q^2 < 0$ and ν correspond to the virtuality of the exchanged boson and its energy in the nucleon rest frame, respectively. Note that $\nu = p \cdot q/M$. It is convenient to introduce a variable

$$y = \nu/E, \tag{3}$$

which measures the ratio of the exchanged boson energy to the incident lepton energy in the nucleon rest frame.

Inelastic lepton-nucleon scattering is related through the one-boson exchange mechanism (see Fig. 2) to the scattering of a virtual boson of "mass" $\sqrt{-Q^2}$ and energy ν on a nucleon. The center-of-mass energy squared of the virtual boson-nucleon scattering is

$$s = (p + q)^2 = -Q^2 + 2M\nu + M^2 \tag{4}$$

and is equal to the square W^2 of the invariant mass of the hadronic system X .

Deep-inelastic scattering corresponds to the region where both ν and Q^2 are large and x is finite and of the order $\mathcal{O}(1)$. The small- x limit of deep-inelastic scattering corresponds to the case in which

$$2M\nu \gg Q^2 \tag{5}$$

$$-q^2 = Q^2 \quad x = \frac{Q^2}{2p \cdot q} = \frac{Q^2}{2M\nu}$$

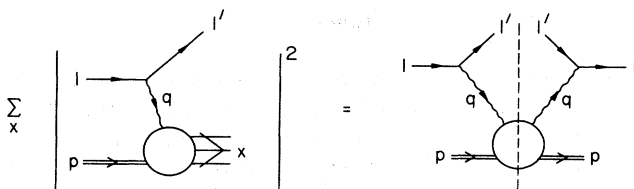


FIG. 2. Kinematics of deep-inelastic scattering and its relation through the optical theorem to Compton scattering for the virtual photon.

yet Q^2 is still large (i.e., at least a couple of GeV^2). The limit $2M\nu \gg Q^2$ is equivalent to $s \gg Q^2$, that is, to the limit when the center-of-mass energy squared, s , is large and much greater than Q^2 . The high-energy limit, when the scattering energy is kept much greater than the external masses (and momentum transfers), is by definition the Regge limit. In deep-inelastic scattering Q^2 is by definition also kept large (i.e., $Q^2 \gg \Lambda^2$, where Λ is the QCD scale parameter). The limit of large ν and $2M\nu \gg Q^2$ is therefore the Regge limit of deep-inelastic scattering (Landshoff and Polkinghorne, 1972). The fact that Q^2 is large allows the use of perturbative QCD.

Low-energy charged-lepton scattering is mediated by a pure electromagnetic interaction. This is also the dominant contribution at low and medium Q^2 at large energies. Therefore it is natural to focus the discussion on one-photon exchange. In this case l and l' in Fig. 2 are leptons of the same kind. The differential cross section is then given by the formula

$$\frac{d^2\sigma(x, Q^2)}{dQ^2 dx} = \frac{4\pi\alpha^2}{Q^4} \left[\left(1 - y - \frac{Mxy}{2E} \right) \frac{F_2(x, Q^2)}{x} + y^2 F_1(x, Q^2) \right], \tag{6}$$

where due to parity conservation only two structure functions, F_1 and F_2 , appear. At much higher Q^2 ($Q^2 \geq M_Z^2$, where M_Z is the Z boson mass) an admixture of the weak interaction (thus axial-vector current) may appear, which introduces a third structure function F_3 (see Charchuła *et al.*, 1990). Thus, when discussing existing deep-inelastic scattering data, we shall mention only the structure functions F_1 and F_2 , except for neutrino scattering data, where the function F_3 will also be referred to. Instead of F_1 the structure function $R(x, Q^2)$ defined as

$$R(x, Q^2) = \sigma_L / \sigma_T = (1 + 4M^2 x^2 / Q^2) F_2 / (2xF_3) - 1 \tag{7}$$

is often used. The differential cross section (6) then reads

$$\frac{d^2\sigma(x, Q^2)}{dQ^2 dx} = \frac{4\pi\alpha^2}{Q^4} \frac{F_2(x, Q^2)}{x} \left[1 - y - \frac{Mxy}{2E} + \frac{y^2(1 + 4M^2 x^2 / Q^2)}{2[1 + R(x, Q^2)]} \right]. \tag{8}$$

Note that, in charged-lepton scattering, $R = \sigma_L / \sigma_T$ where σ_L and σ_T denote the cross sections for longitudinally and transversally polarized virtual photons, respectively. Real photons are only transversally polarized, and therefore σ_L and R vanish when $Q^2 \rightarrow 0$. Within the parton model for quarks of spin $\frac{1}{2}$ (Halzen and Martin, 1984), F_2 depends only on x and is expressed in terms of quark (antiquark) distributions:

$$F_2(x) = x \sum e_i^2 [q_i(x) + \bar{q}_i(x)] \tag{9}$$

and

$$F_2(x) = 2xF_1(x). \tag{10}$$

The last equality (the Callan-Gross relation) gives $R \rightarrow 0$ in the scaling limit. Small nonzero values of R are expected due to the transverse momentum that can arise from the Fermi motion of the quarks inside the nucleon, from radiation of hard gluons by the scattered quark, or from photon-gluon fusion. The longitudinal structure function

$$F_L(x, Q^2) = (1 + 4M^2x^2/Q^2)F_2 - 2xF_1 \tag{11}$$

is related to R via $R = F_L/2xF_1$; F_L is directly sensitive to the gluon distribution function, which plays a crucial role in the interactions at small x .

B. Regge theory

Since the small- x limit of deep-inelastic scattering corresponds to the Regge limit, the concepts of the old Regge theory and Regge phenomenology appear and acquire a new content within perturbative QCD. It may be useful to recapitulate some elements of Regge theory (Collins, 1977), in particular those needed in the description of deep-inelastic scattering at small x .

For a long time it has been known that two-body scattering of hadrons is strongly dominated by small-momentum transfers t or equivalently by small scattering angles. This is successfully described by the exchange of a particle with appropriate quantum numbers. Regge-pole exchange is a generalization of a single-particle exchange (Fig. 3). The Regge poles, like elementary particles, are characterized by quantum numbers like charge, isospin, strangeness, G parity, etc.

The Regge pole carrying the quantum numbers of the vacuum and describing diffractive scattering is called the *Pomeron*. It is related to the Pomernanchuk theorems for asymptotic behavior of total cross sections. Other Regge poles are called *Reggeons*. It is useful to represent Regge-pole exchange in terms of quarks and gluons. Thus the exchange of $q\bar{q}$ bound states (Fig. 4) corresponding to the exchange of mesons can be related to the Regge pole (Reggeon) that carries quantum numbers different from those of the vacuum, while the Pomeron can be thought of as corresponding to an exchange of a pair of gluons. There are no known particles, however, that might be associated with the Pomeron. Note that, in the case of a Regge pole carrying nonzero quantum

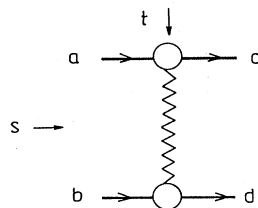


FIG. 3. Regge-pole exchange.

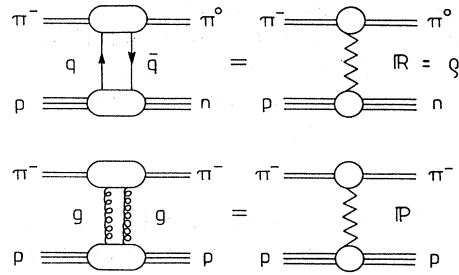


FIG. 4. Quark-exchange (a) and gluon-exchange (b) diagrams and the corresponding Regge-pole exchange for meson-proton scattering. P denotes Pomeron and R Reggeon.

numbers, configurations of the $q\bar{q}$ pairs are possible which cannot be represented by known mesons. Formally the Regge pole corresponds to a pole of the t -channel partial-wave amplitude in the complex angular momentum plane. The position of this pole is described by the trajectory function $\alpha(t)$.

The high-energy behavior of a two-body amplitude due to Regge-pole exchange is

$$A(s, t) \sim s^{\alpha(t)}, \tag{12}$$

where s is the c.m. energy squared of the colliding hadrons. The value of the trajectory function for $t=0$, $\alpha(0)$ is called the *intercept*. The optical theorem relates the imaginary part of the forward (i.e., $t=0$) elastic-scattering amplitude A to the total cross section σ_{tot} :

$$\text{Im } A = s \sigma_{\text{tot}}. \tag{13}$$

Therefore the imaginary part of the forward elastic amplitude gives the high-energy behavior of the corresponding total cross section for the reaction $a + b \rightarrow \text{anything}$. Regge-pole exchange thus gives

$$\sigma_{\text{tot}} \sim s^{\alpha(0)-1}, \tag{14}$$

i.e., the high-energy behavior of the total cross section is controlled by the intercept.

The nonvacuum trajectories of Regge poles associated with the known mesons have intercepts smaller than one [$\alpha_R(0) \approx \frac{1}{2}$ or less], and so the corresponding contributions to the total cross section decrease with increasing energy. In order to describe the energy-independent total cross sections observed at lower energies, one has to assume the intercept of a Pomeron to be equal to 1.

C. Pomeron at high energies

It should be emphasized that the detailed mechanism of high-energy interactions and in particular the nature of the Pomeron may be more complicated than the simple Regge-pole exchange picture. It is therefore more appropriate to speak in general of *Regge singularities*, which may not necessarily be simple poles. The name *Pomeron* is in general a name for the mechanism responsible for diffractive processes at high energies. In partic-

ular, the Pomeron should be able to describe cross sections that increase with the increasing energy.

The increase of the total cross sections with energy (and so the possible nature of the Pomeron) is strongly constrained by the *Froissart bound*, implying that, asymptotically, the total cross sections cannot increase faster than $\ln^2 s$ (Froissart, 1961; Martin, 1982). This bound is a consequence of unitarity and analyticity. It has, in fact, a very simple geometrical content, namely, diffractive scattering can at most correspond to scattering on an expanding black disk with the radius growing not faster than $\ln s$. We stress that this is the asymptotic bound; for finite energies it is possible to have the total cross sections behave (for instance) as $s^{\alpha_p - 1}$ with $\alpha_p > 1$ and still be consistent with unitarity. This behavior, if present, must eventually be slowed down in order not to violate unitarity. We shall discuss this point in more detail now.

When studying the high-energy limit of scattering amplitudes in perturbative quantum field theory, one usually proceeds in two steps: first the *leading $\ln(s)$ approximation*, in which the contributions of those diagrams which at each order n of the perturbative expansion give the maximum power of $\ln(s)$ (usually n) are summed. The sum is called the *bare Pomeron*. Since the leading $\ln(s)$ criterion does not necessarily respect unitarity, one finds in many cases, and as a rule in gauge field theories, that the intercept α_p^B of this bare Pomeron is above unity. The total cross section corresponding to the exchange of this bare Pomeron behaves as $s^{\alpha_p^B - 1}$, i.e., increases as a power of energy for $\alpha_p^B > 1$. This behavior violates the Froissart bound at very high energies. One is then forced to understand how unitarity is restored and to find the appropriate unitarization procedure, which brings the Pomeron back within the unitarity limit. This is the second—and in general much more complicated—step in the analysis of the higher-energy limit. The eikonal model, which treats the bare Pomeron as the eikonal or as the “potential,” may be used in the unitarization procedure (Bourrely *et al.*, 1984a, 1984b, 1988). With the bare-Pomeron intercept above unity, this model leads to diffractive scattering on an expanding black disk and may lead to the saturation of the Froissart bound (Froissart, 1961; Martin, 1982). It should be kept in mind that, within a specific field theory and in particular within the non-Abelian gauge field theories, restoring unitarity may be much more complicated than is implied by application of the simple eikonal prescription (Frolov *et al.*, 1970; White, 1979; Bartels, 1979, 1980).

D. Small x in deep-inelastic scattering on a nucleon

Let us now briefly review the application of Regge theory to deep-inelastic charged-lepton scattering on a nucleon. The natural quantities to consider are the structure functions F_1 and F_2 , which are proportional to the total virtual photon-nucleon cross section (see Sec. II.A

and Fig. 2) and which are expected to have Regge behavior corresponding to Pomeron and/or Reggeon exchange (Landshoff and Polkinghorne, 1972). Let us consider this point in more detail. The virtuality of the exchanged photon is equal to $q^2 = -Q^2$, where $Q^2 > 0$, and the energy of the photon in the laboratory frame (nucleon at rest) is equal to $\nu = pq/M$ (see also Sec. II.A). The invariant mass of the hadronic system produced in γ^*N collision, W , is equal to the total energy in the photon-nucleon c.m. system: $W = \sqrt{s}$. We shall assume that $Q^2 \ll s$, this being equivalent to $2M\nu \gg Q^2$. Applying now the optical theorem to the total cross section for the reaction $\gamma^*N \rightarrow \text{hadrons}$, we introduce the elastic amplitude for the Compton process $\gamma^*N \rightarrow \gamma^*N$ at zero-momentum transfer t between initial and final photons (or initial and final nucleons); see the right side of Fig. 2. At large energies \sqrt{s} and small t , $t \rightarrow 0$, we use the Regge pole or in general the Regge-theory approach to describe this amplitude and then the total cross section [see Eq. (6)]. The predictions obtained in this way for the production of the hadronic system in deep-inelastic scattering can be used to estimate the small- x behavior of the structure functions, since the limit of large $s \gg Q^2$ discussed above corresponds to small $x \sim Q^2/s$.

1. Regge behavior of the structure functions in the parton model

In order to match the Regge behavior of the structure functions with the Bjorken scaling implied by the parton model, one considers the Regge parametrization using the variable $1/x$ instead of s in Eq. (14) (note that $1/x \sim s$ in the limit $s \gg Q^2$). From the Regge behavior of the virtual-photon nucleon total cross sections for transversally and longitudinally polarized photons one gets the following Regge behavior for the structure functions:

$$F_1 \sim x^{-\alpha(0)}, \quad F_2 \sim x^{1-\alpha(0)}, \quad (15)$$

where $\alpha(0)$ is an intercept of the corresponding Regge trajectory.

In the parton model, which is appropriate in large- Q^2 limit, the structure functions are related to the quark and antiquark distributions in the nucleon [see Eq. (9)]. The Regge behavior of the structure function $F_2(x)$ in the large- Q^2 region reflects itself in the small- x behavior of the quark and antiquark distributions. Thus a $1/x$ behavior of the sea-quark and antiquark distributions for small x ,

$$q_{\text{sea}}(x) \sim \frac{1}{x}, \quad (16)$$

corresponds to a Compton amplitude (Fig. 2) with a Pomeron exchange of intercept $\alpha_p = 1$, while a behavior of the valence-quark distributions as $x^{-\alpha_R}$ with $\alpha_R \approx \frac{1}{2}$ corresponds to a mesonic Regge-pole exchange, i.e.,

$$q_{\text{val}}(x) \sim \frac{1}{\sqrt{x}}. \quad (17)$$

The difference between the sea-quark and valence-quark behavior at small x is related to the quantum number exchange in the t channel of the virtual-photon-hadron scattering. The valence-quark distributions stem from the $q\bar{q}$ pair-exchange mechanism, in which the $q\bar{q}$ state can have its quantum numbers different from those of the vacuum. The small- x behavior of the valence-quark distributions is therefore associated with Reggeon exchange. On the other hand, the sea-quark distributions correspond predominantly to the exchange of a $q\bar{q}$ pair carrying vacuum quantum numbers. Their small- x behavior is therefore controlled by Pomeron exchange.¹ Since the same processes lead to gluon and sea-quark distributions in the nucleon, we expect that for small x

$$G(x) \sim \frac{1}{x} \tag{18}$$

The x dependence of the parton densities given above [Eqs. (16)–(18)] is often assumed also for Q^2 -dependent

$$\frac{\partial q_i(x, Q^2)}{\partial \ln(Q^2/\Lambda^2)} = \frac{\alpha_s(Q^2)}{2\pi} \int_x^1 \frac{dy}{y} \left[P_{qq} \left(\frac{x}{y} \right) q_i(y, Q^2) + P_{qG} \left(\frac{x}{y} \right) G(y, Q^2) \right], \tag{19}$$

$$\frac{\partial G(x, Q^2)}{\partial \ln(Q^2/\Lambda^2)} = \frac{\alpha_s(Q^2)}{2\pi} \int_x^1 \frac{dy}{y} \left[\sum_i P_{Gq} \left(\frac{x}{y} \right) q_i(y, Q^2) + P_{GG} \left(\frac{x}{y} \right) G(y, Q^2) \right], \tag{20}$$

where P_{ab} are the one-loop splitting functions. When the appropriate gauge is chosen, the diagrams that contribute in this approximation are the ladder diagrams with gluon and quark exchange (Fig. 5). In those diagrams the longitudinal momenta $\sim x_i$ are ordered along the chain ($x_i \geq x_{i+1}$), and the transverse momenta are strongly ordered (i.e., $k_{\perp, i}^2 \ll k_{\perp, i+1}^2$). It is this *strong ordering* of transverse momenta towards Q^2 which gives the maximal power of $\ln(Q^2)$, since the integration over transverse momentum in each cell is logarithmic (viz., the integrand is proportional to $1/k_{\perp}^2$).

When terms with higher powers of the coupling $\alpha_s(Q^2)$ are included in the right-hand side of Eqs. (19) and (20) one obtains the *next-to-leading logarithmic approximation*. For more details see Charchuła *et al.* (1990).

Let us now look at the small- x limit of the distributions generated by these equations. We note that the term $P_{GG}(z)$ behaves as $6/z$ at small z , which is relevant at small x [see Eqs. (19) and (20), where $z = x/y$]. Retaining in the above equations only these terms, one gets

¹A possible model for the Pomeron exchange, which would give a constant (i.e., energy-independent) cross section and therefore the $1/x$ behavior of the sea-quark distributions, is the two-gluon exchange model (Low, 1975; Nussinov, 1976; Gunion and Soper, 1977).

parton densities at moderate Q^2 . Further discussion of this point is given below.

2. Evolution equations

Let us now discuss the perturbative QCD predictions for the small- x behavior of parton distributions. We shall consider the sea quark and gluon distributions that dominate the valence quarks in the small- x limit. Perturbative QCD becomes applicable in the large- Q^2 region leading to the evolution of the parton densities with Q^2 , expressed in some form of *evolution equations*. The exact form of these equations depends upon the accuracy with which one treats the “large” logarithms $\ln(Q^2/\Lambda^2)$ or $\ln(1/x)$. In the *leading $\ln(Q^2)$ approximation*, which corresponds to keeping only those terms in the perturbative expansion which have the leading power of $\ln(Q^2)$, i.e., $\alpha_s^n \ln^n(Q^2)$, the equations have the familiar form of the *Altarelli-Parisi equations* (Altarelli and Parisi, 1977; Dokshitzer *et al.*, 1980; Reya, 1981; Altarelli, 1982):

the product of maximal powers of *both* large logarithms, $\ln(Q^2)$ and $\ln(1/x)$, which leads to the so-called *double logarithmic approximation*. The powers of $\ln(1/x)$ come from the fact that integration over the longitudinal momentum fraction becomes logarithmic also, and so in the n th order given by the n th iteration of the evolution

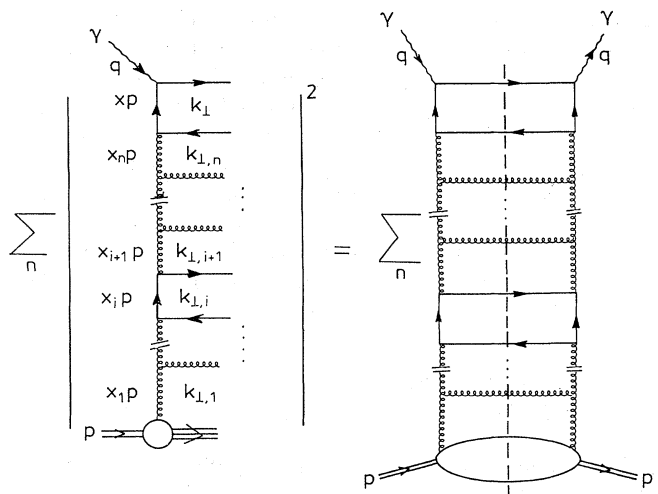


FIG. 5. Ladder diagram for deep-inelastic scattering in the leading $\ln(Q^2)$ approximation.

equations one finds for the gluon at small x

$$G(x, Q^2) \sim \frac{\xi^n(Q^2) \ln^{n-1}(1/x)}{x (n!)^2} \left[1 + O\left(\frac{1}{\ln(1/x)}\right) \right], \quad (21)$$

where

$$\xi(Q^2) = \int \frac{Q^2 dk^2}{k^2} \frac{3\alpha_s(k^2)}{\pi} \sim \ln \ln \left[\frac{Q^2}{\Lambda^2} \right]. \quad (22)$$

The factorials in the denominator of Eq. (21) reflect strong ordering in longitudinal and transverse momenta, respectively. The sum of these terms behaves as

$$xG \sim \exp[2\sqrt{\xi(Q^2)\ln(1/x)}] \times [\text{slowly varying function of } \xi(Q^2)\ln(1/x)] \quad (23)$$

at small x and large Q^2 , i.e., $\xi(Q^2)\ln(1/x) \gg 1$. This predicts that in the small- x limit the gluon distribution (multiplied by x) will grow faster than any power of $\ln(1/x)$. The same applies to the sea quarks, since the dominant contribution to sea-quark distributions at small x comes from the $q\bar{q}$ pairs emitted from gluons (Fig. 6).

The double logarithmic approximation does not, however, take into account all leading terms in the parton densities in the small- x limit. By definition it neglects

$$f(x, k^2) = f^0(x, k^2) + \frac{3\alpha_s(k^2)}{\pi} k^2 \int_x^1 \frac{dx'}{x'} \int_{k_0^2}^{\infty} \frac{dk'^2}{k'^2} \left\{ \frac{f(x', k'^2) - f(x', k^2)}{|k'^2 - k^2|} + \frac{f(x', k^2)}{\sqrt{4k'^4 + k^4}} \right\}, \quad (24)$$

where the function $f(x, k^2)$ is the nonintegrated gluon distribution, i.e.,

$$f(x, k^2) = \frac{\partial xG(x, k^2)}{\partial \ln k^2}, \quad (25)$$

$f^0(x, k^2)$ is a suitably defined inhomogeneous term, k^2, k'^2 are the transverse momenta squared of the gluon in the final and initial states, respectively, and k_0^2 is the lower-limit cutoff. The important point here is that, unlike the case of the leading $\ln(Q^2)$ approximation, the transverse momenta are *no longer* ordered along the chain. As before the dominant contribution to sea-quark distributions comes from the $q\bar{q}$ pairs emitted from

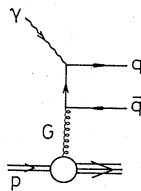


FIG. 6. Sea-quark distribution related to the gluon distribution in deep-inelastic scattering.

terms in the perturbative expansion that contain the leading power of $\ln(1/x)$ but are not accompanied by the leading power of $\ln(Q^2)$.

The sum of leading powers of $\ln(1/x)$ [and arbitrary powers of $\ln(Q^2)$] corresponds to the *leading $\ln(1/x)$ approximation* (Kuraev *et al.*, 1977; Balitskij and Lipatov, 1978; Gribov *et al.*, 1983; Ciafaloni, 1988; Catani *et al.*, 1990a, 1990b). This approximation is equivalent to the leading $\ln(s)$ approximation. The equivalence of the leading $\ln(s)$ and leading $\ln(1/x)$ approximations follows from the fact mentioned above that in the limit $s \gg Q^2$, $x \sim Q^2/s$, and so $\ln(1/x) \sim \ln(s/Q^2)$. This approximation gives the bare Pomeron in perturbative QCD. The diagrams that contribute in this approximation are ladderlike, but the exchange mechanism along the ladder is slightly more complicated. Instead of the elementary gluon exchange, one has the exchange of the *Reggeized gluon* (Fig. 7). The term “Reggeized gluon” means that one can associate with the gluon the Regge trajectory that is calculable in perturbative QCD (Kuraev *et al.*, 1977; Balitskij and Lipatov, 1978; Bronzan and Sugar, 1978; Lipatov and Szymanowski, 1980; Gribov *et al.*, 1983; Levin, 1991).

The *Balitskij-Lipatov equation*, which sums these diagrams, has the form (Balitskij and Lipatov, 1978; Bronzan and Sugar, 1978; Gribov *et al.*, 1983; Kwieciński, 1985a; Levin, 1991)

gluons (Fig. 6).

When the running of the QCD coupling is neglected [i.e., when one sets $\alpha_s(Q^2) = \alpha_0$] the Balitskij-Lipatov equation can be solved analytically, and one obtains at

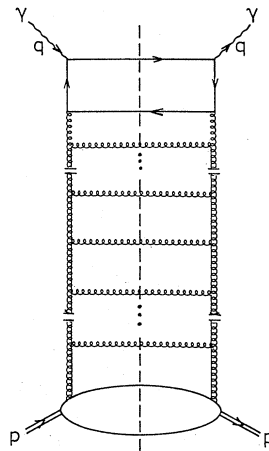


FIG. 7. Ladder diagram for deep-inelastic scattering in leading $\ln(1/x)$ approximation, with gluon exchanges reggeized along vertical lines.

small x

$$xG(x, Q^2) \sim \frac{x^{1-\alpha_p^B}}{(\ln x)^{1/2}} \left[1 + O\left(\frac{1}{\ln x}\right) \right], \quad (26)$$

where

$$\alpha_p^B = 1 + \frac{12\alpha_0}{\pi} \ln 2 \quad (27)$$

corresponds to the intercept of the bare QCD Pomeron, which in this approximation describes the fixed (i.e., t -independent) branch-point singularity. It should be noted that it can have a potentially large magnitude, e.g., $\alpha_p^B > \frac{3}{2}$ for a typical value of $\alpha_0 = 0.2$. When running coupling-constant effects are taken into account, this fixed branch-point singularity turns into an infinite number of Regge poles (Cardy, 1974, 1975; Lipatov and Szymanowski, 1980) where positions are controlled by $\alpha_s(k_0^2)$. The small- x behavior of parton distributions is now

$$xG(x, Q^2) \sim x^{1-\alpha_p^B}, \quad (28)$$

where α_p^B denotes the intercept of the leading (i.e., the rightmost) pole. Again this can be large, $\alpha_p^B \approx \frac{3}{2}$ (Lipatov, 1986; Collins and Kwieciński, 1989), as in the fixed-coupling case.

It is also possible to generalize the leading $\ln(1/x)$ equation in a way that treats both large logarithms, i.e., $\ln(Q^2)$ and $\ln(1/x)$, on an equal footing (Gribov *et al.*, 1983; Levin, 1991). The numerical study of these equations suggests, however, that the results do not differ substantially from the solution of the conventional Altarelli-Parisi equations, at least in the region of not-too-small values of $x > 10^{-4}$ (Kwieciński, 1985b; Charchuła and Krawczyk, 1990; Krawczyk, 1990; Marchesini and Webber, 1991, 1990).

These considerations summarize the properties of the bare perturbative QCD Pomeron. The validity of the various approximations depends upon the regions of x and Q^2 , as presented in Fig. 8. Since this problem is re-

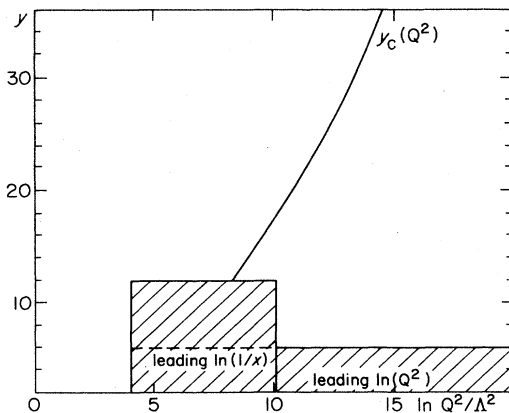


FIG. 8. Regions of applicability of different approximations and the definition of the critical line, which here corresponds to the large- Q^2 asymptotic form $y_c(Q^2) = (1/4c)\ln^2(Q^2/\Lambda^2)$, where $c = 12/(11 - 2n_f/3)$ with the number of flavors n_f set to 4 (Kwieciński *et al.*, 1991a, 1991b).

lated to the screening corrections, it will be considered below.

The above discussion dealt with purely perturbative QCD results. Possible nonperturbative effects (i.e., those generated by the nonperturbative modification of the gluon propagators coming from the gluon condensate) on small- x behavior are discussed by Landshoff and Nachtmann (1987), Cudell *et al.* (1989), and Donnachie and Landshoff (1989).

3. Screening corrections

The unlimited increase of the parton distributions (multiplied by x) leads to a conflict with unitarity, i.e., too rapid increase of high-energy cross sections violating the Froissart bound (Froissart, 1961; Martin, 1982). The violation of the Froissart bound and its possible restoration can be understood within a simple geometrical picture (Gribov *et al.*, 1983; Levin, 1991), which we shall now describe. To this end let us first note that the quantity $xG(x, Q^2)$ is equal to the number of gluons n_G in the nucleon per unit of rapidity $y = \ln(1/x)$ having a transverse size $\sim 1/Q$. This follows from the fact that the function $G(x, Q^2)$ is, by definition, the number density of gluons in a nucleon, i.e.,

$$G(x, Q^2) = dn_G(x, Q^2)/dx, \quad (29)$$

and so

$$xG(x, Q^2) = dn_G/d \ln(1/x) = dn_G/dy. \quad (30)$$

Unfortunately we have no direct deep-inelastic scattering type of measurement with photonic or W/Z probes for gluons. There does exist, however, a strong-interaction analog to deep-inelastic scattering, which is the hadron-nucleon interaction in which a highly virtual gluon from a hadron probes the structure of the nucleon. So, for the moment, let us consider the interaction of an external hard gluonic probe G^* of virtuality $0 > q^2 = -Q^2$ with a nucleon.

Within the QCD improved parton model, when one counts incoherently the individual probe-gluon cross sections, the cross section corresponding to the virtual gluon-nucleon interaction (per unit of rapidity) is

$$\sigma_{G^*N} = \sigma_0 xG(x, Q^2), \quad (31)$$

where σ_0 is the total cross section corresponding to the interaction of the probe with the gluon in a nucleon, i.e.,

$$\sigma_0 = \sigma_{G^*G \rightarrow X} = \text{const} \frac{\alpha_s(Q^2)}{Q^2}. \quad (32)$$

The increase of the gluon distributions in the manner described in the previous sections would violate the Froissart limit for the cross section σ_{G^*N} as well as for other hadronic cross sections.

We are now in a position to see that the violation of the Froissart bound can be interpreted in simple geometric terms. Let us assume that the cross section σ_0

is equal to the transverse area of the probed parton. Since $xG(x, Q^2)$ denotes the number of small- x gluons, the right-hand side of Eq. (31) is equal to the area occupied by the small- x gluons in a nucleon. Since the number of gluons, xG , can grow indefinitely for $x \rightarrow 0$, Eqs. (23), (26), and (28), the total transverse area occupied by gluons can become comparable to or larger than the transverse area of a nucleon, πR^2 , for sufficiently small values of x and/or Q^2 . This effect is called in the literature *parton overcrowding*. When this happens (and in fact before this happens), gluons begin to overlap spatially in the transverse direction and interact. This means that they can no longer be treated as free partons (Gribov *et al.*, 1983; Levin, 1991). This is in conflict with the basic assumption of the QCD improved parton model, in which the partons are assumed to be noninteracting. The formula for the cross section must therefore be modified accordingly. The interaction of partons should be expected to tame the indefinite increase of parton distributions in the small- x limit in such a way that the total cross section becomes equal to the geometrical one, i.e., equal to πR^2 . When this limit is reached, one speaks of *parton saturation*.

We shall now briefly discuss how this picture is quantitatively realized in QCD. Clearly the crucial parameter here is \mathcal{W}_{sat} defined as

$$\mathcal{W}_{\text{sat}}(x, Q^2) = \frac{\sigma_0 x G(x, Q^2)}{\pi R^2}. \quad (33)$$

In the region of x and Q^2 , where $\mathcal{W}_{\text{sat}} \ll 1$, we are in the limit of applicability of the QCD improved parton model, and the parton evolution with Q^2 proceeds along the lines described in the preceding section. The QCD evolution described by Eqs. (19) and (20)—and corresponding to the ladder diagram—is the evolution of the individual partonic cascades. The important point here is that the interaction of partons from different cascades can be neglected.

When $\mathcal{W}_{\text{sat}} \sim \alpha_s(Q^2)$, then partons from different cascades begin to overlap spatially (transversely) and interact. This interaction of partons leads to nonlinear screening (or shadowing) corrections to the evolution equations (19) and (20).

In the simplest version, the corrected evolution equation takes the form (Gribov *et al.*, 1981a, 1981b; Mueller and Qiu, 1986)

$$\begin{aligned} & \frac{\partial xG(x, Q^2)}{\partial \ln Q^2} \\ &= \frac{3\alpha_s(Q^2)}{\pi} \int_x^1 \frac{dy}{y} [yG(y, Q^2)] \\ & \quad - \frac{9}{16R^2} \left[\frac{3\alpha_s(Q^2)}{Q} \right]^2 \int_x^1 \frac{dy}{y} [yG(y, Q^2)]^2. \end{aligned} \quad (34)$$

In this equation the linear term on the right-hand side was obtained from the standard evolution equation for gluons [Eq. (20)] by neglecting the quark contribution

and keeping only the most singular term of the $P_{GG} \sim 6/z$. That means that, in fact, $G(x, Q^2)$ is treated here in the double logarithmic approximation. The second term in Eq. (34) is the screening correction. Note that this equation is written for $G(x, Q^2)$ times x . The origin of the negative sign of the screening correction will be discussed in Sec. II.F.

The modified evolution equation (34) makes our discussion of the screening effect more quantitative. In particular, the parameter \mathcal{W}_{sat} can be defined here to be equal to the ratio of the integrands of the second and first terms on the right-hand side of Eq. (34). This leads to the following expression for the parameter \mathcal{W}_{sat} :

$$\mathcal{W}_{\text{sat}} = \frac{27\pi\alpha_s(Q^2)}{16R^2 Q^2} xG(x, Q^2). \quad (35)$$

The screening term may also contain terms with higher powers of the gluon distributions (Mueller, 1990a). Taking into account the quadratic term alone, as in Eq. (34), is justified only when the nonlinear corrections are relatively small.

The main role of the nonlinear screening term in Eq. (34) is to tame the indefinite increase of $xG(x, Q^2)$ in the small- x limit. One finds that for $x \rightarrow 0$ the gluon distribution obtained in this way approaches the so-called *parton saturation limit* $G^{\text{sat}}(x, Q^2)$ (Gribov *et al.*, 1983; Collins and Kwieciński, 1989; Bartels, 1991; Levin, 1991):

$$xG^{\text{sat}}(x, Q^2) = \frac{16}{27\pi\alpha_s(Q^2)} R^2 Q^2, \quad (36)$$

which corresponds to $\mathcal{W}_{\text{sat}} = 1$ in Eq. (35). Before this limit is reached, however, one expects that higher-order terms of the screening corrections, as well as other contributions, will become important. In some models these higher-order contributions modify the saturation limit by a factor that is a slowly varying function of x (Mueller, 1990a). In the region of x and Q^2 , where $\mathcal{W}_{\text{sat}} \sim 1$, non-perturbative confinement effects can also become important.

The most dramatic consequence of parton saturation is a *linear scaling violation* in parton distributions [see Eq. (36)] to be contrasted with the mild logarithmic scaling violation given by perturbative QCD.

The evolution equation (34) is expected to hold in the region where $\mathcal{W}_{\text{sat}} \leq \alpha_s(Q^2)$, i.e., below the so-called *critical line* (Fig. 8) (Gribov *et al.*, 1983; Bartels, 1991; Levin, 1991), where $\mathcal{W}_{\text{sat}} \sim \alpha_s(Q^2)$. For large Q^2 ,

$$y_c(Q^2) = \frac{11 - 2n_f/3}{48} \ln^2 \frac{Q^2}{\Lambda^2} \quad (37)$$

in the $(y = \ln 1/x, \ln Q^2)$ plot, where n_f denotes the number of flavors. A complete discussion of the origin of the critical line would require introduction of the so-called “semiclassical approximation” of the evolution equation, which is too technical and therefore avoided here. The details concerning this point are presented by Gribov *et al.* (1983), Bartels (1991), Kwieciński *et al.* (1991a,

1991b), and Levin (1991).

The magnitude of the *radius parameter* R controlling the strength of the screening corrections is expected to be smaller than the magnitude of the *hadronic radius*. This comes from the fact that two diagrams can contribute to the shadowing term (Fig. 9). The magnitude of the contribution in Fig. 9(a) (when the gluonic ladders forming the gluon distribution are attached to the different constituents of a hadron) is controlled by the hadronic radius, while the contribution of the diagram in Fig. 9(b) (when the ladders are attached to the same constituent) is controlled by the much smaller *constituent radius*. If the second contribution prevails, as advocated by Levin and Ryskin (1990a, 1990b), then one obtains the so called “hot spots” picture of a hadron, in which the gluons are packed within regions much smaller than the hadronic size (Gribov *et al.*, 1983; Mueller, 1990b; Levin, 1991). In this model, screening (shadowing) is very important, and parton saturation can be reached for values of x and Q^2 that are accessible at HERA (Bartels *et al.*, 1990, 1991; Kwieciński *et al.*, 1990; Mueller, 1990b; Bartels, 1991).

4. Types of parton parametrizations

The existing experimental data for moderately large values of Q^2 (e.g., $Q^2 > 5 \text{ GeV}^2$) do not provide very strong constraints on the behavior of parton distributions in the very-low- x region. The accessible values of x are $x \geq 10^{-2}$, where the shape of the parton distribution is still to a large extent controlled by terms that are non-leading in the small- x limit. The main message from QCD analysis is that small- x behavior, particularly in the region of moderately large values of Q^2 , is very sensitive to the boundary conditions at some reference Q_0^2 scale, and the results can differ by an order of magnitude or even more.

The conventional assumption has been that the gluon and quark sea distributions should have a $1/x$ behavior at small x and for moderately large values of the reference scale Q^2 (see Sec. II.D.1). The increase of the parton distributions (multiplied by x), and so the increase of the structure function $F_2(x, Q^2)$ for Q^2 not far from the reference scale (i.e., for $Q^2 \approx 10\text{--}20 \text{ GeV}^2$ or so), is then still rather slow. This comes from the fact that the evolution parameter $\xi(Q^2)$, which controls the increase in the small- x region [see Eq. (22)], is still small. The screening corrections were also estimated for this class of distributions and found to be relatively small (i.e., $< 20\%$;

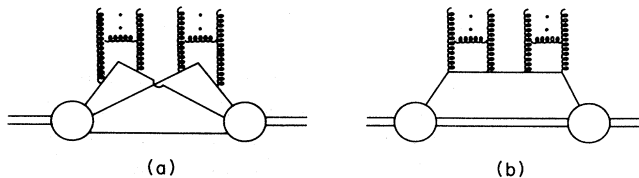


FIG. 9. Shadowing terms (a) with $R = R_H$ and (b) for the hot spots picture with $R = R_{\text{parton}}$ (from Kwieciński *et al.*, 1990).

Kwieciński, 1985b). These conventional distributions can become negative when evolved “backwards” to scales $Q^2 < Q_0^2$. One can argue, however, that the “leading twist” approximation, which neglects terms proportional to $1/Q^2$, it is not applicable in this region.

Positivity of the parton distributions down to very low values of Q^2 can be achieved through less conventional input parametrizations, which for moderately large values of Q^2 predict a steep rise in the parton distributions with decreasing x . Such, for instance, are the *radiatively generated parton distributions* (Reya, 1981; Glück *et al.*, 1988, 1989; see Sec. II.G). They start from the pure valence-quark distributions at the very low scale $Q_0^2 \approx 0.06 \text{ GeV}^2$ [for $Q_0^2 \approx 0.2 \text{ GeV}^2$ and some “valence” gluons in the new formulation of the model (Glück *et al.*, 1990, 1991)]. In another example, approximate effects of the bare QCD Pomeron are included in parton distributions in the form of the $x^{-3/2}$ behavior of the input sea-quark and gluon distributions at the scale $Q_0^2 \approx 5 \text{ GeV}^2$ (Kwieciński *et al.*, 1990). In the former case the very steep increase of the parton distributions with decreasing x is caused by the relatively large magnitude of the evolution parameter $\xi(Q^2)$, while in the latter case the increase is the direct consequence of the input. In both cases the calculated gluon distributions can overcome their saturation limit at $x > 10^{-4}$ and moderately large values of Q^2 , and so the screening corrections can no longer be neglected as in the case of distributions that originated from “ $1/x$ ” input. The screening corrections can indeed be very important, since they could reduce the magnitude of the gluon distributions by a factor as large as 2.5–3 for $x \approx 10^{-4}$ (Collins and Kwieciński, 1990).

Most QCD analyses go beyond the leading $\ln(Q^2)$ approximation, taking into account also the next-to-leading terms in the evolution kernels. They are dependent upon the renormalization scheme, leading to scheme-dependent parton distributions. The most frequently used is the modified minimal subtraction ($\overline{\text{MS}}$) scheme (Tung, 1989). In this scheme the next-to-leading term in the gluon-quark splitting function becomes singular at small x , enhancing the sea quarks at the expense of gluons. These effects can be partly compensated by changes in the value of the QCD scale parameter Λ (Tung, 1990). As has been discussed, for example, by Charchuła *et al.* (1990), one cannot directly compare parton distributions obtained in different schemes or parton distributions belonging to the leading $\ln(Q^2)$ approximation with those of the next-to-leading $\ln(Q^2)$ type.

Recently three next-to-leading-order QCD analyses were performed (Glück, Reya, and Vogt, 1990, 1991; Kwieciński, Martin, Roberts, and Stirling, 1990; Morfin and Tung, 1991), in which special attention was paid to the small- x behavior of the parton distribution functions. In particular, Kwieciński *et al.* incorporated both the singular $x^{-3/2}$ type of behavior of the gluon and sea-quark distributions and shadowing effects into their parametrization. In Sec. IV we discuss the predictions for HERA based on these parametrizations.

E. Deep-inelastic diffraction

The *deep-inelastic diffractive process* related to deep-inelastic scattering is defined as

$$l + N \rightarrow l' + X + N, \quad (38)$$

with a large rapidity gap between the nucleon in the final state and the produced system X . The production mechanism in this case is expected to be dominated by Pomeron exchange (Fig. 10). In the large- Q^2 region one is therefore probing the *parton content of a Pomeron* (Fig. 11; Donnachie and Landshoff, 1984, 1987; Ingelman and Schlein, 1985; Berger *et al.*, 1987; Ryskin, 1988, 1990; Streng, 1988; Bartels and Ingelman, 1990; Ingelman, 1990; Nikolaev and Zakharov, 1992).

Concerning the partonic structure of the Pomeron, it is usually assumed that it consists predominantly of gluons (Donnachie and Landshoff, 1984, 1987; Ingelman and Schlein, 1985; Berger *et al.*, 1987; Streng, 1988). In this approach the parton distributions are assumed to be normalized by the ordinary momentum conservation sum rules saturated by gluons. Various forms of gluon distributions in a Pomeron have been considered; the experimental data on jet production within the diffractively produced system seem to favor “soft” parametrization (Bonino *et al.*, 1988). In this model the quark distributions within the Pomeron are generated radiatively from gluons as the effect of QCD evolution. On the other hand, in the papers by Donnachie and Landshoff (1984, 1987; see also Ingelman and Schlein, 1985, Berger *et al.*, 1987, and Streng, 1988) it is assumed on the basis of the Pomeron-photon analogy that the Pomeron couples predominantly to quarks. In this approach the quark distributions are not constrained to satisfy the momentum conservation sum rules. The very interesting possibility was considered by Ryskin (1988, 1990), by Bartels and Ingelman (1990), and recently by Nikolaev and Zakharov (1992) that deep-inelastic diffraction can be calculated almost entirely within perturbative QCD from triple gluonic ladder diagrams, i.e., from the same diagrams that describe parton screening effects in the modified evolution equations discussed in Sec. II.D.3. Theoretically this problem is strongly connected with the calculation in QCD of the fundamental quantity describing (large-mass) diffraction, i.e., the so-called triple Pomeron vertex. Again the parton distributions calculated within this

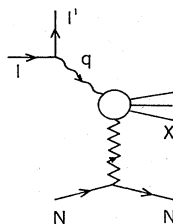


FIG. 10. Deep-inelastic diffraction. The zigzag line represents a Pomeron.

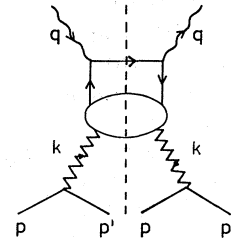


FIG. 11. Pomeron structure function in deep-inelastic diffraction.

purely perturbative model are not constrained to satisfy the momentum conservation sum rules. In general momentum conservation sum rules give parton distributions of relatively large magnitude in a Pomeron.

F. Low- x nuclear physics

In the last decade abundant experimental data on the structure of a nucleon in a nuclear environment have become available. The bound-nucleon structure is interesting in itself, but an understanding of it also permits extraction of the free-nucleon structure function from the nuclear data. This has important practical consequences, especially for neutrino scattering experiments in which luminosity limitations exclude the use of hydrogen targets. In what follows, $F_2(A)$ and $R(A)$ shall denote *bound-nucleon structure functions* or the structure functions of a nucleus A normalized to the number of nucleons. In particular, $F_2(\text{H})$ is the structure function of a proton (sometimes also denoted F_2^p), and $F_2(\text{D})$ is the structure function of a nucleon (obtained from a deuteron neglecting its weak binding). The same convention will be applied to a cross section $\sigma(A)$.

It is known that the bound-nucleon structure function $F_2(A)$ differs substantially from that measured for free nucleons $F_2(\text{D})$ (Frankfurt and Strikman, 1988), a still controversial phenomenon called the *EMC effect* after the European Muon Collaboration who first observed it (Aubert *et al.*, 1983). The most intriguing and (quantitatively) rather poorly understood part of this effect, the reduction of $F_2(A)$ for $x < 0.1$, has been known for a long time as *nuclear shadowing* (Bauer *et al.*, 1978; Grammer and Sullivan 1978; Covolan and Predazzi, 1991). Shadowing describes a phenomenon in which the reaction cross section per nucleus is less than A times the single-nucleon cross section. This phenomenon is studied by comparing the cross sections (structure functions) per nucleon from nuclear and nucleon targets. Deuterium is traditionally taken as a free-nucleon target in the experiments (Arnold *et al.*, 1984; Bari *et al.*, 1985; Ashman *et al.*, 1988; Arneodo *et al.*, 1990, 1988; Amaudruz *et al.*, 1991b). Nuclear interactions can be described using the partonic language exclusively. However, in certain circumstances it might be easier to use the nucleon degrees of freedom as well.

Nuclear shadowing effects in the large- Q^2 region where the parton model is applicable are expected to reflect shadowing at the parton level in the nucleus. In a simple space-time picture of the interaction of the virtual probe with the nuclear target, shadowing sets in when the longitudinal size of a parton having a certain momentum fraction x , $\Delta z_p = 1/xp$ exceeds the Lorentz contracted distance between two neighboring nucleons in the nucleus, $\Delta z_N = 2r_N M/p$ (p is nucleon momentum, $r_N \sim 1$ fm), in the reference frame in which the nucleus is sufficiently rapid. This means that partons' longitudinal dimensions extend over more than one nucleon, possibly over the whole nucleus. If their transverse dimensions $b = 1/Q$ are similar, then such partons may overlap spatially and recombine. This leads to the suppression of the parton density for values of x smaller than a certain value $x_A = 1/2Mr_N \approx 0.1$ (shadowing) and possibly to the enhancement of the parton distributions at $x > x_A$ (antishadowing), i.e., to a redistribution of the parton momenta. Thus, at sufficiently small x , the partons (quarks and/or gluons) in a nucleus are not independent, as is assumed in the parton model; that is, the cross section for hard scattering will not grow linearly with A . Shadowing will disappear very slowly with increasing Q^2 . The interaction of partons from different nucleons, leading to a reduction of the effective number of partons in a nucleus, is the basic mechanism of shadowing in nuclear parton distributions in perturbative QCD (Nikolaev and Zakharov, 1975; Mueller and Qiu, 1980; Qin, 1987). In the region of very small values of x ($x \ll 1/2MR_A$ where R_A is the nuclear radius), shadowing effects can be enhanced by partons overcrowding in a nucleon, as implied by perturbative QCD (Gribov *et al.*, 1983; Levin, 1991; see discussion in Sec. II.D.3).

To quantify the above mechanism of nuclear shadowing, one can represent the interaction of the virtual photon with the nucleus in the form of a *multiple-interaction series*. Different terms of the series correspond to different numbers of nucleons in a nucleus participating in the interactions (see Fig. 12). For a deuteron, for example, one has two such terms. The corresponding structure function is related via the optical theorem to the imaginary part of the amplitude from Fig. 12. The first diagram gives the sum of all structure function of protons and neutrons. Shadowing comes from the second and higher terms, when more than one nucleon participate in the interaction. The different models of shadowing correspond to different structural details of these diagrams. In what follows we shall limit our discussion to double scattering.

The shadowing contribution to the sum of structure functions of all nucleons is negative. Two possible origins of this negative sign are discussed in the literature.

(1) The “conventional” origin, which corresponds to the dominant imaginary amplitude describing individual virtual-photon–nucleon interactions in double scattering. This is essentially the same as the origin of the negative

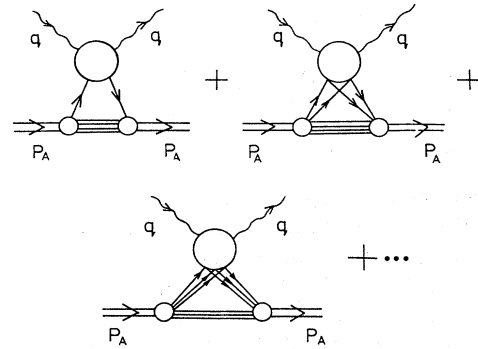


FIG. 12. Multiple-scattering expansion for the virtual-photon–nucleus scattering amplitude. The solid lines correspond to the probe and nucleons in a nucleus (from Kwieciński, 1990).

sign of the Glauber double-scattering term in hadron-nucleus interactions (see Franco and Glauber, 1966) when the hadron-nucleon scattering amplitudes are predominantly imaginary. This “conventional” approach is usually combined with Pomeron exchange in the multiple-interaction mechanism (Kwieciński and Badełek, 1988; Kwieciński, 1990; Badełek and Kwieciński, 1992). Almost all models of shadowing belong to this class, e.g.,

(i) the model based on the theory of inelastic screening adapted to deep-inelastic scattering on nuclear targets. This allows the shadowing corrections in parton distributions on a nucleon target and to parton distributions in the Pomeron (Kwieciński and Badełek, 1988; Zoller, 1992a, 1992b; Badełek and Kwieciński, 1992). Multiple scattering of the diffractively produced system within a nucleus can also be taken into account in a model-dependent way (Kwieciński, 1990);

(ii) the aligned-jet model in which the virtual probe is assumed to dissociate into a $q\bar{q}$ pair of limited p_{\perp} (i.e., the virtual-photon-aligned “jet”), which in turn interacts within the nucleus with a “typical hadronic” cross section (Frankfurt and Strikman, 1989). Absorptive rescattering of this pair within a nucleus leads to shadowing (Nikolaev and Zakharov, 1991);

(iii) the model in which the virtual photon is assumed to dissociate into a $q\bar{q}$ pair and shadowing is a consequence of a subsequent antiquark-nucleus multiscattering process (Brodsky and Lu, 1990).

The shadowing term in perturbative QCD is given by the multiple exchange of gluon ladders coupling to the $q\bar{q}$ pair in the upper part of the diagram shown in Fig. 13. In the case of a two-ladder exchange diagram, the negative sign comes from the fact that each amplitude corresponding to the QCD ladder is predominantly imaginary. Different cuts (i.e., diagrams in which either zero, one, or two ladders are cut) give different contributions to the imaginary part of the amplitude, corresponding to the diagram of Fig. 13. Cuts between the ladders [diffractive

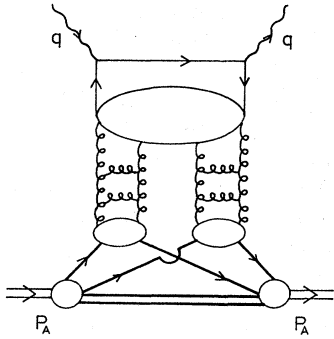


FIG. 13. Two-gluon ladder exchange for the double-interaction diagram. The upper blob denotes different perturbative QCD couplings of the four gluons to the $q\bar{q}$ pair.

production, Fig. 14(a)] and through both of them [part of the nondiffractive production, Fig. 14(b)] give a positive contribution. The contribution is negative when the cut goes through one of the ladders [nondiffractive production with absorption, Fig. 14(c)]. A cut through both ladders (Fig. 15) may be related to perturbative QCD *parton recombination processes* that modify the parton evolution (Nikolaev and Zakharov, 1975; Mueller and Qiu, 1986).

(2) An alternative explanation of the negative sign of the shadowing term uses the probabilistic “gain and loss” arguments when considering the effects of parton fusion on their momentum distributions (Close *et al.*, 1989; see Fig. 16). Shadowing corresponds to the negative “loss” term, while the “gain” term leads to a positive antishadowing contribution in the large- x region ($x > 0.1$), i.e., the momentum sum rule is unchanged.

The first approach leads to shadowing effects in the small- x region, while the antishadowing has to be added as a separate phenomenon. In contrast to this, in the second approach the antishadowing results from parton fusion, and the negative “loss term” has to be added as a separate contribution to balance the momentum. It would certainly be very interesting to understand the possible relation between these two approaches and to show that the “loss term” can be related to the double scattering corresponding to absorptive amplitudes. It should be noted that in both cases one encounters the parton recombination mechanism, yet their details are significantly different. It is therefore misleading to refer to a single “recombination” mechanism without specifying which of the cases (1) or (2) one has in mind. To be precise, the genuine perturbative QCD recombination effects which modify the parton evolution involve radiatively produced partons (Fig. 15). On the other hand, the shadowing effects considered by Close *et al.* (1989) correspond to recombination of partons in the initial state (Fig. 16). Within the QCD evolution formalism this initial-state recombination may be regarded as a possible model for the shadowing corrections to the input parton distributions which have to be provided before evolution. In fact, most of the analyses performed so far imply that

the magnitude of shadowing depends essentially upon the magnitude of the input, see, for example, Mueller (1990a). An extensive review of shadowing is that of Colan and Predazzi (1991).

G. Low- x , low- Q^2 phenomena

As will be shown in the next section, in the presently available data coming from both nucleon and nuclear tar-

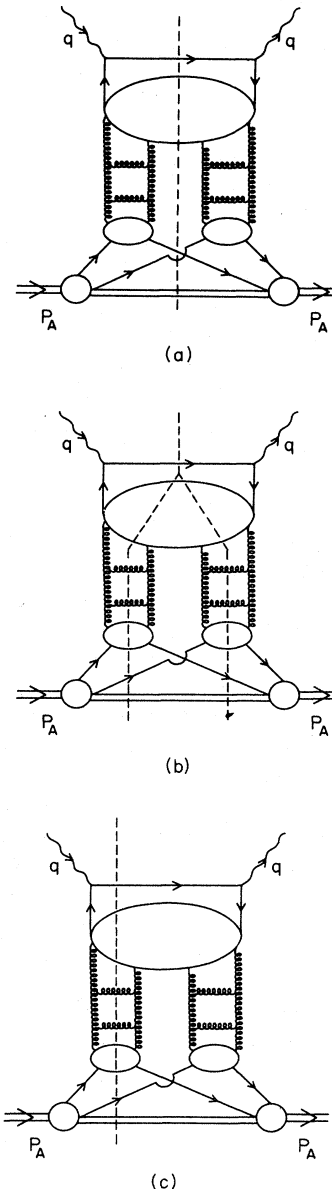


FIG. 14. Cuts of the two-gluon ladder exchange diagrams: (a) diffractive production accompanying breaking of the nucleus; (b) nondiffractive production on both nucleons; (c) nondiffractive production on one nucleon followed by absorptive corrections on the other nucleon. There exists a symmetric diagram in which the second ladder is cut instead of the first one.

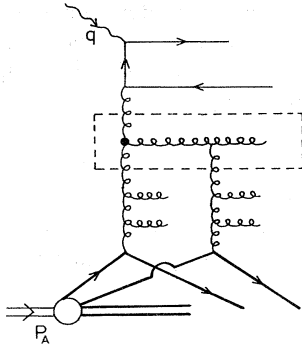


FIG. 15. Possible contribution to the diagram from Fig. 14(b). The box illustrates the recombination of two gluons coming from different nucleons.

gets the lowest x values correspond to the region of low Q^2 , $Q^2 < 1 \text{ GeV}^2$ i.e., the nonperturbative region. Therefore we shall briefly summarize the current knowledge of low- Q^2 phenomena. This will be done using “traditional” approaches. Some of the results for $Q^2 \sim 0$ can also be obtained in a different way, using the concept of the photon structure function (Abramowicz *et al.*, 1991b).

Due to conservation of the electromagnetic current, F_2 must vanish as Q^2 goes to zero. Also $R \rightarrow 0$ in this limit (see Sec. II.A). This implies that scaling should not be a valid concept in the region of very low Q^2 . The exchanged photon is then almost real, and the close similarity of real photonic and hadronic interactions justifies the use of the vector-meson-dominance (VMD) concept (Bauer *et al.* 1978; Grammer and Sullivan, 1978) for the description of F_2 . In the language of perturbation theory, this concept is equivalent to a statement that a physical photon spends part of its time as a “bare,” pointlike photon and part as a virtual hadron or hadrons. In the simplest form of VMD, the hadronic component is identified with the vector mesons ρ , ω , and ϕ . The interplay between the hadronic behavior of the virtual photon (dominating at low Q^2) and its pointlike electromagnetic interaction (dominating at high Q^2) can be studied through the measured Q^2 dependence of the structure functions in a wide range of Q^2 values. For a more detailed discussion of the high-energy photon-hadron interaction, including not only the VMD component but also pure partonic contributions to the physical photon state, see Abramowicz *et al.* (1991b).

It is desirable to have a theoretical scheme capable of

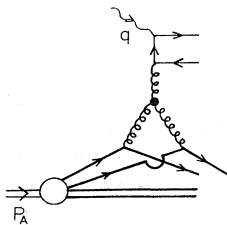


FIG. 16. “Initial-state” fusion of gluons from different nucleons in a nucleus.

including in a consistent way both photon interaction mechanisms, independently of the involved value of Q^2 . One possible scheme is provided by the generalized vector-meson-dominance model (GVMD) (Bauer *et al.*, 1978; Grammer and Sullivan 1978), which is an extension of the parton model ideas into the low- Q^2 region. Apart from GVMD there exist several phenomenological parametrizations extrapolating the structure functions from the scaling region to low values of Q^2 (Stein *et al.*, 1975; Gordon *et al.*, 1979; Donnachie and Landshoff, 1984; Abramowicz, Levin, Levy, and Maor, 1991). Although very useful, they lack the dynamical content of GVMD.

The GVMD model is based on a dispersion-relation-like representation of structure functions in Q^2 for fixed (large) s , with $s \gg Q^2$, where $s = W^2$. This representation is approximated by the contribution of (an infinite number of) vector mesons which couple to virtual photons (Fig. 17). In this traditional formulation the GVMD model contains several ambiguities, such as the choice of spectrum for the vector mesons (or parametrizations of the large- Q^2 part), magnitude of possible nondiagonal terms, scaling violation effects, etc. Below we shall give two examples of the *nucleon* structure-function calculations which extend over the low- Q^2 region.

An example of a model based on the GVMD representation of F_2 is that developed by Kwieciński and Badełek (1989). In this model the large- Q^2 part of the corresponding discontinuity was directly obtained by an analytic continuation of the structure function from the scaling region, instead of its decomposition into possible contributions from (large-mass) vector mesons. This procedure not only avoided some of the above-mentioned ambiguities of the traditional GVMD model, but also allowed to obtain a representation of the structure function that permitted studies of the effect of scaling violation in the large- Q^2 region on the low- Q^2 part of the structure function. It was shown that the magnitude of the partonic contribution to F_2 can be as large as 50% of the vector-meson contribution in the low- Q^2 , low- x region. At the same time, the increase of the quark sea in the limit $x = 0$ at large Q^2 , implied by QCD, was found to be rather weak at low Q^2 .

In the quantitative QCD calculations of the low- x structure function done by Glück, Godbole, and Reya (1988, 1989; see also Sec. II.D.4) the starting point for the moment evolution was taken as $Q^2 = \mu^2 = (0.25 \text{ GeV})^2 \simeq (M/3)^2$, where valence quarks were assumed to be the only partons existing in the nucleon at the scale μ^2 (the “static point”). The generated parton distributions are well defined and positive, but they rise steeply with decreasing x , much more so than the conventionally cal-

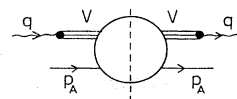


FIG. 17. The generalized vector-meson-dominance representation for Compton scattering.

culated distributions (e.g., Diemoz *et al.*, 1988). In a new version of the model a number of “valencelike” gluons are also present at the initial scale, and the steep growth of the parton distributions at low x is tamed (Glück *et al.*, 1990, 1991).

The natural and probably dominant mechanism of *nuclear shadowing* at low Q^2 and in photoproduction is the multiple scattering of vector mesons, which couple to photons (Bauer *et al.*, 1978; Grammer and Sullivan 1978; Covolan and Predazzi, 1991; Badełek and Kwieciński, 1992; see Fig. 18). Assuming that the vector-meson–nucleon amplitude is predominantly imaginary, one obtains immediately a negative sign of shadowing corrections, as in the Glauber model with predominantly imaginary amplitudes. This mechanism of shadowing does, therefore, belong to case (1) of Sec. II.F. The space-time picture of the interaction is now as follows: at sufficiently high photon energies the hadronic fluctuation of the photon may travel a distance exceeding the nuclear diameter $2R_A$. A virtual photon will then interact with the nucleus like an ordinary hadron. In the rest frame of the nucleus, the propagation distance for a photon in the hadronic state of mass M_h is

$$\Delta d \sim \frac{1}{\Delta E} = \frac{2\nu}{Q^2 + M_h^2}, \quad (39)$$

where ΔE is the difference between the energy ν of the virtual photon and E_h of the hadron of the same momentum. In the VMD picture, the condition for the onset of shadowing is that $\Delta d > 2r_N$ (assuming that the h - N cross section is large enough), where $r_N \sim 1$ fm is the distance between two neighboring hadrons in the nucleus. From Eq. (39) one sees that the shadowing of a particular hadronic state M_h will vanish when ν is small and Q^2 is large. This last condition corresponds to $Q^2 \gg M_h^2$, since M_h^2 is equal to 0.5–1 GeV² for the ρ , ω , and Φ mesons. When $Q^2 \gg M_h^2$, then $\Delta d \sim 1/Mx$ and the condition for the onset of shadowing can be expressed in terms of the Bjorken scaling variable only: $x < x_A = 1/2Mr_N \simeq 0.1$, which is the same value as that obtained in the fast-nucleus reference frame, Sec. II.F.

Several VMD-based models have been proposed to explain nuclear shadowing effects (Bilchak *et al.*, 1988, 1989; Piller *et al.*, 1989; Shaw, 1989), applying hadronic language to describe the deep-inelastic scattering at $x < 0.1$ at low and moderate Q^2 . The models include both the low-mass vector mesons and the continuum of the $q\bar{q}$ states in the photon, the former contribution accounting for the low- Q^2 region of the shadowing

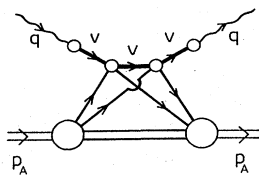


FIG. 18. Double scattering of vector mesons.

phenomenon. These models are reviewed by Covolan and Predazzi (1991). Multiple scattering of vector mesons that couple to the virtual photons was considered in a formalism in which shadowing was related to the inclusive diffractive processes (Kwieciński and Badełek, 1988; Badełek and Kwieciński, 1992).

III. EXPERIMENTS IN THE LOW- x REGION

Where the parton model is applicable (i.e., for $Q^2 > 3$ GeV² or so), small values of x can be measured only in high-energy (high- ν) experiments. However, for the existing fixed-target experiments, the low- x , high- ν condition can only be obtained at the expense of lowering Q^2 below 1 GeV². This in turn means that the outgoing lepton is scattered at very small angles, usually equal to a few milliradians, i.e., practically within the lepton beam divergence limits. Therefore the selection and reconstruction of the events in the small-angle scattering experiments involve triggers, trigger processors, and software systems that are much more sophisticated than those normally used in deep-inelastic scattering experiments. Moreover, the extraction of the inelastic single-photon exchange cross section (or extraction of the structure functions) from the data requires corrections of the experimental yield for the radiative processes, i.e., separating the cross section due to the reaction in Fig. 2 from the higher-order electromagnetic and weak effects faking the interesting events and distorting experimental distributions. Radiative processes may account for a substantial part of the measured low- x cross section, especially for nuclear targets.

This section is a survey of small- x experiments up to the present. The experiments are listed, then a method of extracting structure functions from the measurements is given, together with a more detailed discussion of radiative corrections. Finally an up-to-date collection of the small- x results is presented.

A. List of experiments

Listed below are the experiments providing the presently available low- x ($x < 0.03$) data referenced later in this paper. The ranges of x and Q^2 covered by some of the high-energy experiments are displayed in Fig. 19. Observe the strong correlations between these ranges.

1. Muon (electron) scattering experiments

(1) The Cambridge-Chicago-Illinois-Oxford (CHIO) Collaboration experiment performed at the Fermilab accelerator with 96, 147, and 219-GeV muons scattering off hydrogen and 147-GeV muons off deuterium. The structure function F_2 was measured for $0.0005 < x < 0.7$, $0.2 < Q^2 < 80$ GeV² and R for $0.003 < x < 0.10$, $0.4 < Q^2 < 30$ GeV² (Gordon *et al.*, 1979). Observe that in this experiment low values of x were obtained by using

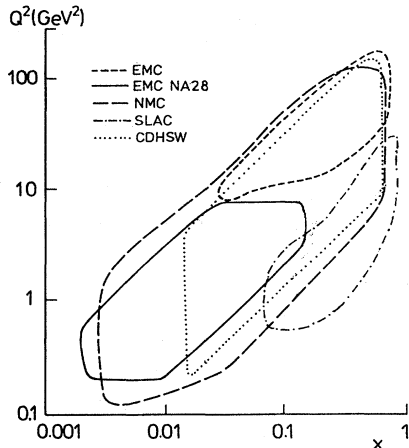


FIG. 19. Acceptance regions in some deep-inelastic scattering experiments on deuterium. For comparison the CDHSW acceptance for $\nu(\bar{\nu})$ -Fe scattering is also shown.

data at high values of y , where systematic effects are most significant (see Sec. III.B).

(2) A dedicated, low-scattering-angle experiment numbered NA28 performed by the European Muon Collaboration (EMC) at the CERN SPS with a positive muon beam of nominal energy 280 GeV. Structure functions F_2 were measured on deuterium, carbon, and calcium targets for $0.002 < x < 0.17$ and $0.2 < Q^2 < 8$ GeV² (Arvidson *et al.*, 1986; Arneodo *et al.*, 1990, 1988).

(3) The New Muon Collaboration (NMC), experiment, performed at the CERN SPS with muon beams of energies 90, 120, 200, and 280 GeV. The target materials were ¹H, ²D, ⁴He, ⁶Li, ¹²C, ⁴⁰Ca, ⁵⁶Fe, ¹²⁰Sn, ²⁰⁸Pb, and the kinematical range of measurements was: $0.006 < x < 0.6$, $0.8 < Q^2 < 75$ GeV² for $F_2(\text{H})$ and $F_2(\text{D})$ (Bird *et al.*, 1991); $0.003 < x < 0.7$, $0.12 < Q^2 < 100$ GeV² for the ratio $F_2(\text{D})/F_2(\text{H})$ (Allasia *et al.*, 1990; Amaudruz *et al.*, 1991a; Brüll *et al.*, 1991; Amaudruz *et al.*, 1992a); $0.007 < x < 0.8$, $0.6 < Q^2 < 18.3$ GeV² for the $F_2(\text{Ca})/F_2(\text{Li})$, $F_2(\text{C})/F_2(\text{Li})$, and $F_2(\text{Ca})/F_2(\text{C})$ ratios (Amaudruz *et al.*, 1992b); and $0.0035 < x < 0.65$, $0.5 < Q^2 < 90$ GeV² for the $F_2(\text{He})/F_2(\text{D})$, $F_2(\text{C})/F_2(\text{D})$, and $F_2(\text{Ca})/F_2(\text{D})$ (Amaudruz *et al.*, 1991b). The bulk of the data is still being analyzed.

(4) The experiment of the E665 Collaboration under way at FNAL using a 490-GeV positive muon beam and ¹H, ²D, ¹²C, ⁴⁰Ca, ¹³¹Xe, ²⁰⁸Pb targets. Preliminary results for the $F_2(\text{Xe})/F_2(\text{D})$ structure-function ratio at Q^2 down to 0.01 GeV² and x down to 0.0002 have been presented (Halliwell *et al.*, 1991; Jaffe *et al.*, 1991; Schellman *et al.*, 1991).

Several low-energy electroproduction experiments have been performed on both hydrogen and nuclear targets (see Franz *et al.*, 1981, for a comprehensive review of the results). In particular, extensive studies were carried out from 1970 to 1985 at SLAC using a variety of targets [experiments E49a (Poucher *et al.*, 1974, 1973), E61 (Stein *et al.*, 1975), E87 (Bodek *et al.*, 1979, 1983),

E139 (Arnold *et al.*, 1984), and E140 (Dasu *et al.*, 1988a, 1988b)]. The data were recently reanalyzed (Whitlow, 1990; Whitlow *et al.*, 1990; Bodek *et al.*, 1991) using the improved versions of the radiative correction procedure and were normalized to those from the high-precision experiment E140. The reanalysis permitted extraction of $R(x, Q^2)$ and $F_2(x, Q^2)$ for proton and deuteron over the range $0.1 < x < 0.9$, $0.6 < Q^2 < 20$ GeV² (Whitlow, 1990; Whitlow *et al.*, 1990; Bodek *et al.*, 1991).

2. Neutrino scattering experiments

(1) The Caltech-Columbia-FNAL-Rochester-Rockefeller (CCFRR) Collaboration measured the neutrino (antineutrino)-iron scattering in the FNAL quadrupole-focused beam of energies 120, 140, 168, 200, and 200 GeV (MacFarlane *et al.*, 1984). F_2 and $x F_3$ were extracted for $0.015 < x < 0.65$ and $1.3 < Q^2 < 200$ GeV². New, precise results in the kinematic limits extending to higher Q^2 at high x were presented recently by the Chicago-Columbia-FNAL-Rochester-Wisconsin (CCFR) Collaboration (Mishra *et al.*, 1991).

(2) The CERN-Dortmund-Heidelberg-Saclay-Warsaw (CDHSW) Collaboration performed a neutrino (antineutrino)-iron scattering experiment at the CERN SPS using the wide-band beam of energy up to about 280 GeV. Measured were F_2 , $x F_3$ for $0.015 < x < 0.65$, $0.19 < Q^2 < 196$ GeV² and F_L , $\bar{q}\bar{\nu}$ in somewhat narrower Q^2 intervals (Berge *et al.*, 1991).

(3) The Big European Bubble Chamber (BEBC) Collaboration at CERN measured the neutrino (antineutrino)-deuteron interaction using the wide-band beam of energy up to 200 GeV. Both F_2 and $x F_3$ isoscalar functions were measured in the range $0 < Q^2 < 64$ GeV², $0.028 < x < 0.7$ on neon in BEBC (Varvell *et al.*, 1987; Guy *et al.*, 1987).

B. Extraction of the structure functions, radiative corrections, and systematic errors

In muon (electron) scattering experiments usually only the scattered lepton was measured, while in neutrino-induced reactions a measurement of the final-state hadronic energy was also performed. The bulk of the low- x experimental data comes from muon scattering experiments. Neutrino measurements are limited in this region by poor experimental resolution. Thus we shall concentrate on the muon data unless we state otherwise.

The inelastic cross section (8), denoted by σ_{inel} , is expressed in terms of the two structure functions $F_2(x, Q^2)$ and $R(x, Q^2)$. The function $R(x, Q^2)$ is determined using measurements of the cross section at different beam energies. Experimental information on R is scarce (see Sec. III.C.1), and in order to determine F_2 from Eq. (8) one needs to make various assumptions concerning the behavior of R over a wide range of x and Q^2 values (see below).

It is traditionally assumed that R is independent of the nuclear mass. This is consistent with the current experimental data at higher values of x (Whitlow, 1990; Whitlow *et al.*, 1990; Bodek *et al.*, 1991). The A independence of R implies that the ratio of cross sections measured in targets 1 and 2, σ_1/σ_2 , is equal to the structure-function ratio, $\sigma_1/\sigma_2 = F_2^1/F_2^2$.

Knowing $R(x, Q^2)$, one extracts $F_2(x, Q^2)$ from the data in an iterative process: the events are Monte Carlo simulated assuming the F_2 parametrization and taking into account the radiative corrections and apparatus inefficiencies. The extracted values of F_2 are weakly sensitive to the assumed values of R when the data are restricted to small y values, say $y < 0.5$.

As mentioned earlier, extracting F_2 at small x depends crucially on excluding the background from the higher-order electromagnetic and weak processes accounting for a large fraction of the measured cross section σ_{meas} . These higher-order corrections comprise radiation of real photons by the incoming or outgoing muon [Fig. 20(a),(b)], vertex and vacuum polarization corrections [Fig. 20(c),(d)], two-photon exchange [Fig. 20(e)], hadron current correction [Fig. 20(f),(g)], and electroweak effects. Of these, the radiative processes of Fig. 20(a),(b),(c),(d) contribute significantly to σ_{meas} . They change the kinematics and the experimental resolution of the deep-inelastic scattering event [Fig. 20(a),(b)] or modify the flux of the virtual photons [Fig. 20(c),(d)].

To evaluate the radiative processes, one needs detailed information on nuclear structure (nuclear and nucleon form factors, as well as models for calculating suppression due to the Pauli exclusion principle). Observe that calculations require $\sigma_{\text{inel}}(x, Q^2)$, i.e., $F_2(x, q^2)$ and $R(x, Q^2)$ in the region

$$x_{\text{meas}} < x < 1 \text{ and } 0 < Q^2 < Q^2(x=1, \nu_{\text{meas}}) ;$$

see Fig. 21.

As an example in Fig. 22 the radiative correction factor, $\eta = \sigma_{\text{inel}}/\sigma_{\text{meas}}$, is shown as a function of y [cf. Eq. (3)] for different values of x . Calculations were performed for the muon-deuteron and muon-calcium scattering at 280-GeV incident muon energy. The method of Mo and Tsai (1969) and Tsai (1971) was used

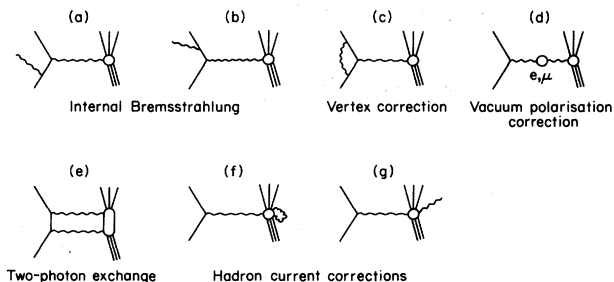


FIG. 20. Some lowest-order and second-order contributions to the radiative corrections. From Sloan *et al.* (1988).

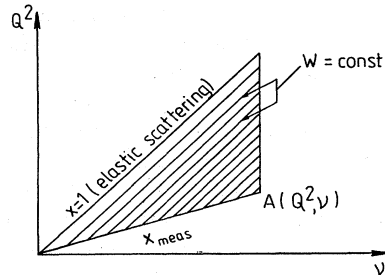


FIG. 21. Kinematic region in which the cross section must be known in order to compute the radiative corrections to the inelastic cross section at point A .

to calculate σ_{meas} (Lietzke and Wimpenny, 1989).

Radiative processes indeed give a predominant contribution to σ_{meas} at low x , especially at large y and for heavy nuclear targets. Most important here are those photon bremsstrahlung reactions [Fig. 20(a),(b)] in which the muon-nucleon interaction is coherent. One way of decreasing this background is to use the information from the hadron vertex (Fig. 2) measurements. In the radiative correction calculations for HERA, defining Q^2 from the lepton and x from the hadron vertex seems to be the best solution (Feltesse, 1992). Calorimetric measurements of the radiative photons may also provide a useful constraint.

The calculations of the radiative processes were checked experimentally by the EMC in two consecutive measurements of bremsstrahlung photons for $0.006 < x < 0.1$ and high values of y (Aubert *et al.*, 1981,1984). A reasonable agreement between the calculations and the data was obtained. A further check was made on the EMC NA28 results, in which the ν dependence of a fraction of events containing no secondary tracks and coming from the μCa and μD interactions was studied (Arneodo *et al.*, 1988, 1990). The observed be-

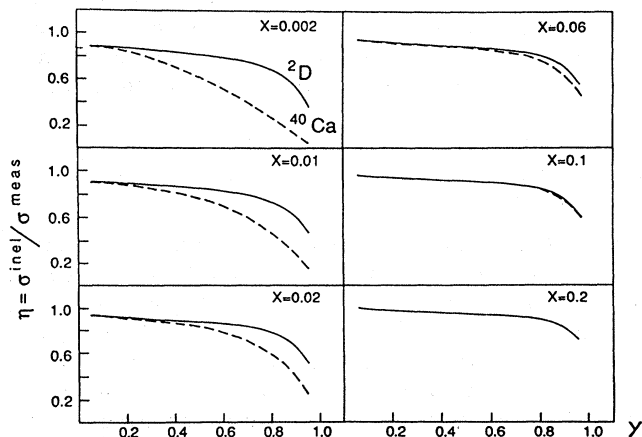


FIG. 22. Radiative correction factors obtained for deuteron (solid curves) and for calcium (dashed curves). From Arvidson *et al.* (1987).

havior agreed with that expected from the radiative processes within the errors, after allowance for the conversion of photons and acceptance effects.

In addition to the early work of Mo and Tsai, a much more detailed scheme developed by the Dubna group (Akhundov *et al.*, 1977, 1986; Bardin and Shumeiko, 1979; Lohmann and Akhundov, 1990) is also used for radiative correction calculations (Sloan *et al.*, 1988). Although there are significant differences in how the different factors are calculated in these two methods, the effects tend to cancel out, and no discrepancy between the resulting radiative correction factors η are noticeable except perhaps a few-percent difference in the large- x , large- Q^2 region (Lietzke and Wimpenny, 1989) due to electroweak effects that are neglected in the Mo and Tsai treatment. Therefore large- Q^2 measurements (e.g., at HERA) should be radiatively corrected using the Dubna scheme, since in this region the electroweak effects are much more significant.

The largest systematic uncertainties in small-angle scattering experiments come from the trigger and software reconstruction inefficiencies; see, for example, the results of EMC NA28 (Arneodo *et al.*, 1988, 1990). In the complementary target experiment of NMC (Al-lasia *et al.*, 1990; Amaudruz *et al.*, 1991a, 1991b), most of these uncertainties cancel in the structure-function ratios, and the dominant systematic error at low x comes from uncertainties in the calibration of the (incoming and outgoing) muon momentum, in the position of the interaction vertex, and in the radiative corrections (information on nuclear structure, accuracy of the method, etc).

C. Results of the low- x structure-function measurements

Only a few sets of deep-inelastic scattering data extend to $x < 0.03$. The reader should be warned that these data sets are obtained under different assumptions. For example, structure functions $F_2(x, Q^2)$ are extracted assuming different values of $R(x, Q^2)$, or systematic errors (especially normalization) are not always included in the final results. In neutrino-scattering analysis, the treatment of heavy-quark contribution effects is often not the same for different data sets.

1. $R(x, Q^2)$

Recent CDHSW measurements of $R(x, Q^2)$ together with other high- Q^2 experimental results are shown in Fig. 23 (Berge *et al.*, 1991). The CDHSW results are consistent with $R = 1.5(1-x)^4/\ln(Q^2/\Lambda^2)$, $\Lambda = 0.2$ GeV. Comparison with the SLAC E140 points is given in Fig. 24. All data indicate a small value of R at moderate values of x and an increase of R with decreasing x , compatible with QCD predictions. These predictions depend on the knowledge of $F_2(x)$ and of the gluon distribution function $G(x)$, and may therefore differ for different input quark and gluon distributions. In the old CHIO

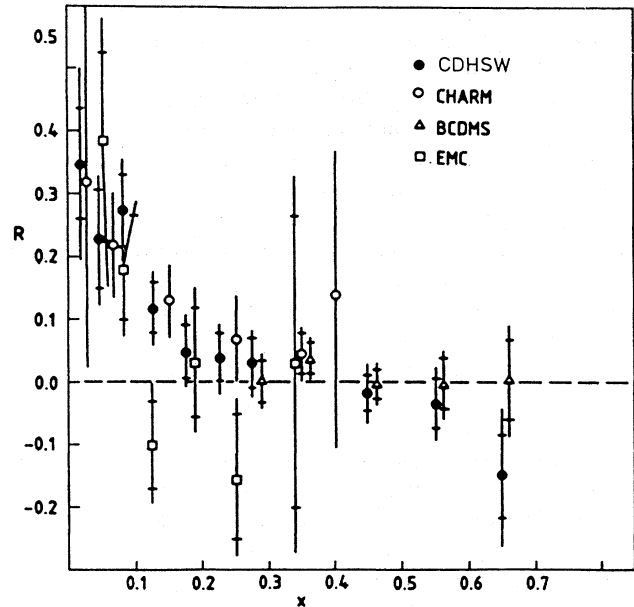


FIG. 23. Recent CDHSW measurements of the $R(x, Q^2)$ together with other high- Q^2 results. From Berge *et al.* (1991).

measurements (Gordon *et al.*, 1979), due to the large errors, the data were consistent with both a constant value of R : $R = 0.52 \pm 0.35$ and R varying with x and Q^2 , as suggested by QCD: $R = R_0(1-x)/Q^2$ or $R = R'_0(1-x)/\ln(Q^2/\Lambda^2)$, $R_0 = 1.20^{+0.43}_{-0.30}$, $R'_0 = 1.18^{+0.39}_{-0.33}$ when $\Lambda = 0.5$ GeV.

At HERA the ability to change the beam energies between 15 and 30 GeV and 300 and 820 GeV for electrons and protons, respectively, will provide an opportunity for

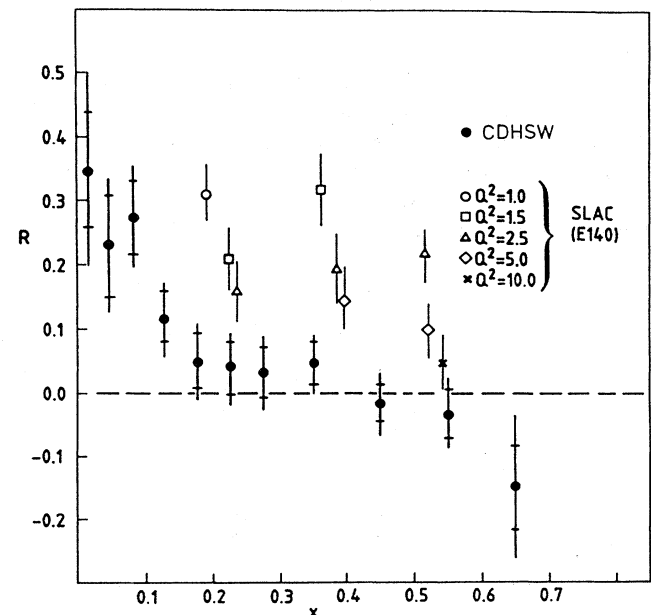


FIG. 24. CDHSW measurements of the $R(x, Q^2)$ compared with the SLAC E140 points. From Berge *et al.* (1991).

statistically precise measurements of R down to $x \sim 10^{-3}$ or so (Fig. 25; Blümlein *et al.*, 1988).

2. Nucleon structure functions from hydrogen and deuterium

The results for the nucleon structure function obtained from deuterium in the dedicated EMC NA28 experiment, $F_2(D)$, are presented in Figs. 26 and 27 as a function of x and Q^2 (Arneodo *et al.*, 1990, 1988). In addition to the errors marked on the figures there is an overall normalization error of 7%. Values of the coefficients of the function fitted to the data and the numerical values of $F_2(D)$ are given in Arneodo *et al.* (1990, 1988). In the analysis the CHIO parametrization of R , $R = R_0(1-x)/Q^2$ (Gordon *et al.*, 1979), was used (for the NA28 data y was smaller than 0.6, and therefore the results were not too sensitive to assumptions about R).

No significant x dependence is visible in any Q^2 interval for $Q^2 < 3 \text{ GeV}^2$ (Fig. 26). This means that the increase of the structure function coming from the increase of the quark sea in the limit of small x , implied by QCD at higher Q^2 , is relatively weak at low Q^2 . For larger Q^2 , the data are shifted towards the higher x values due to the experimental acceptance, and the x dependence observed in deep-inelastic scattering emerges. This pattern is confirmed when comparing the data coming from SLAC (Poucher *et al.*, 1974, 1973; Bodek *et al.*, 1979, 1983), CHIO (Gordon *et al.*, 1979), and the EMC measurements at low angles (Arneodo *et al.*, 1990, 1988) (Fig. 28).

The Q^2 dependence of $F_2(D)$ is shown in Fig. 29. Once systematic errors are taken into account there is reasonable agreement of the NA28 results with the SLAC data (Poucher *et al.*, 1974, 1973; Bodek *et al.*, 1979, 1983) at lower Q^2 , and with the CHIO (Gordon *et al.*, 1979) and EMC measurements at higher Q^2 (Aubert *et al.*, 1987).

In addition, a relative normalization correction of 8% between the data of Stein *et al.* (1975), Poucher *et al.* (1974, 1973), Bodek *et al.* (1979, 1983), and Aubert *et al.* (1987) is necessary. The data in Fig. 29 are therefore consistent with linear variation of $F_2(D)$ with $\log Q^2$ at both low and high Q^2 . This means that a similar scale-breaking pattern to that observed at high Q^2 (Aubert *et al.*, 1987) holds in the range of moderate Q^2 . Since NA28 found F_2 to be constant with x for $x < 0.1$, the values were averaged over x in this range. Figure 30 shows the mean value of F_2 for $x < 0.1$ as a function of Q^2 in linear [Fig. 30(a)] and logarithmic [Fig. 30(b)] scales in Q^2 , as measured by the NA28 experiment. The data extrapolate well to $F_2=0$ at $Q^2=0$, as expected from the conservation of the electromagnetic current.

The data are reasonably well reproduced by the GVMD-based model (Kwieciński and Badełek, 1989), Fig. 31, which has no free (fitted) parameter. However, the comparison should be treated only qualitatively due to the lack of an asymptotic structure function reliable in a wide interval of x , which is necessary in the GVMD calculations [Kwieciński and Badełek (1989) used a parametrization based on the old neutrino data (Eichten *et al.*, 1984)]. The radiatively generated structure function (Glück *et al.*, 1988, 1989) overshoots the data points

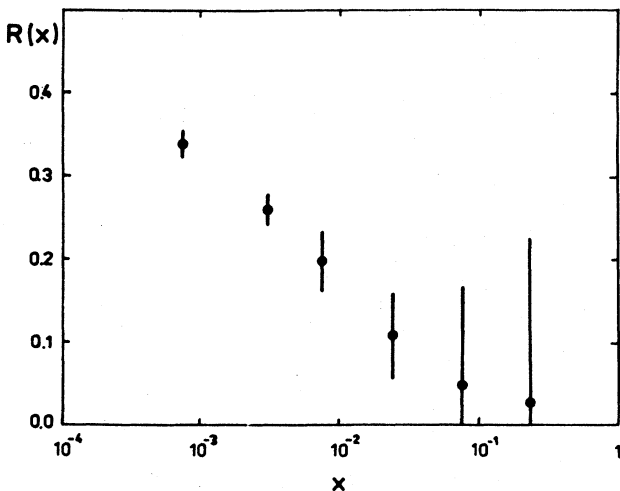


FIG. 25. Measurements of the $R(x, Q^2)$ planned at HERA. From Blümlein *et al.* (1988).

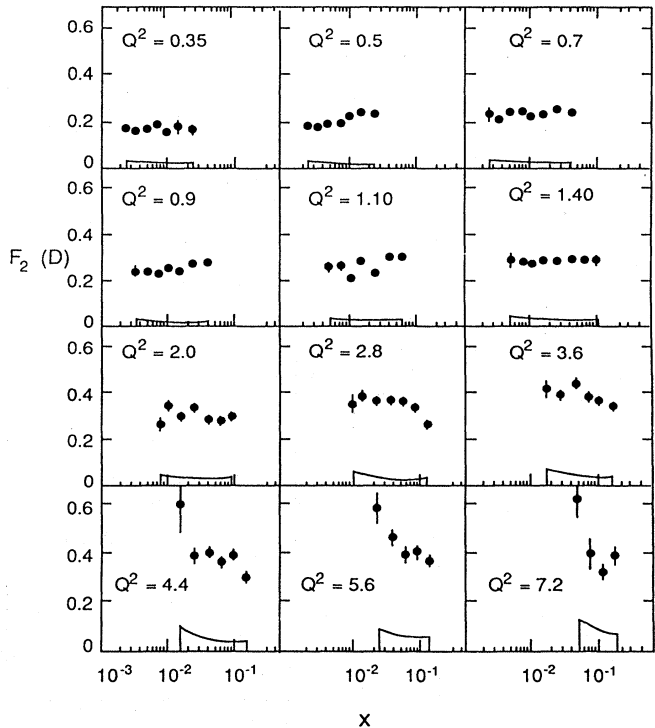


FIG. 26. Nucleon structure function $F_2(D)$ obtained by EMC NA28 from deuterium as a function of x for different intervals of Q^2 (in GeV^2). Statistical errors are indicated by bars; systematic errors are shown by the bands beneath. In addition to the marked errors there is an overall normalization error of 7% (from Arneodo *et al.*, 1990, 1988).

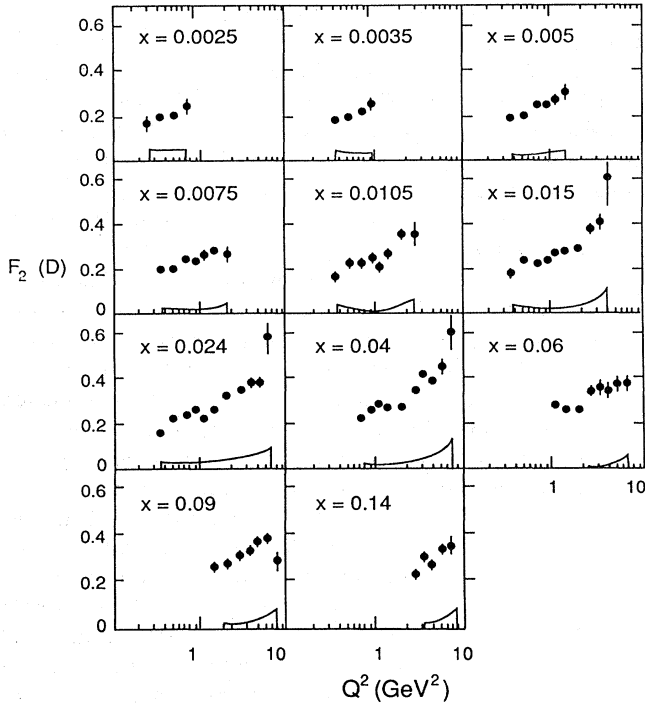


FIG. 27. Nucleon structure function $F_2(D)$ obtained by EMC NA28 from deuterium as a function of Q^2 (in GeV^2) for different intervals of x . Errors as in Fig. 26 (from Arneodo *et al.*, 1990, 1988).

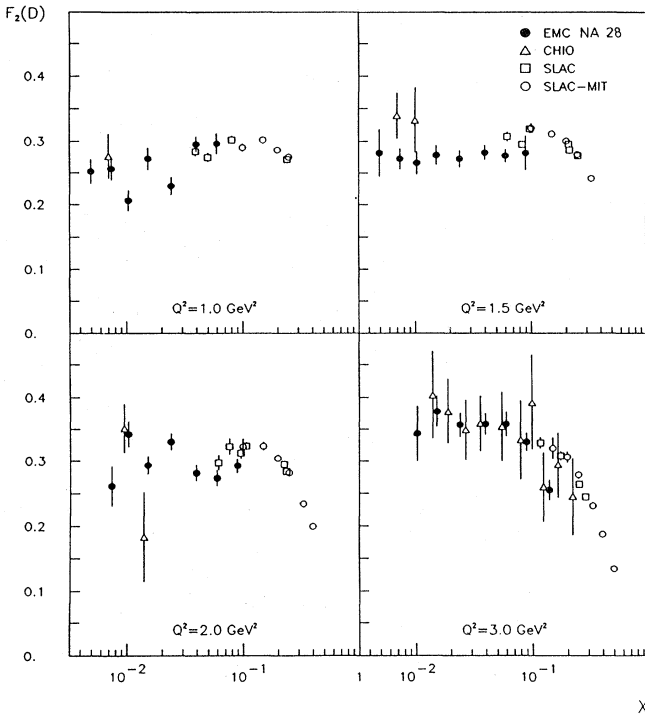


FIG. 28. Nucleon structure function $F_2(D)$ obtained by EMC NA28 from deuterium as a function of x for different intervals of Q^2 (in GeV^2) compared to the results of CHIO (Gordon *et al.*, 1979), SLAC (Poucher *et al.*, 1974, 1973), and SLAC-MIT (Bodek *et al.*, 1979, 1983). Errors are statistical (from Arneodo *et al.*, 1990, 1988).

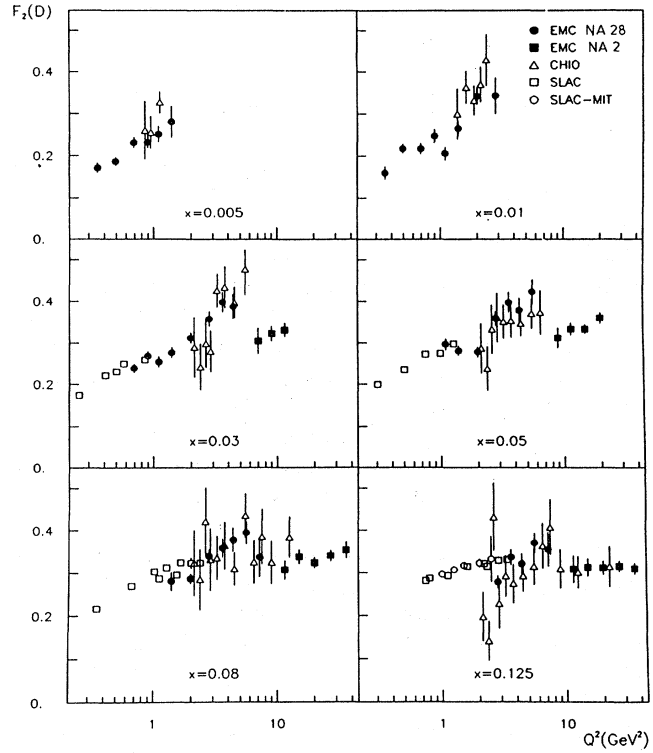


FIG. 29. Nucleon structure function $F_2(D)$ obtained by EMC NA28 from deuterium as a function of Q^2 (in GeV^2) for different intervals of x , compared to the results of EMC (Aubert *et al.*, 1987), CHIO (Gordon *et al.*, 1979), SLAC (Poucher *et al.*, 1974, 1973), and SLAC-MIT (Bodek *et al.*, 1979, 1983). Errors are statistical (from Arneodo *et al.*, 1990, 1988).

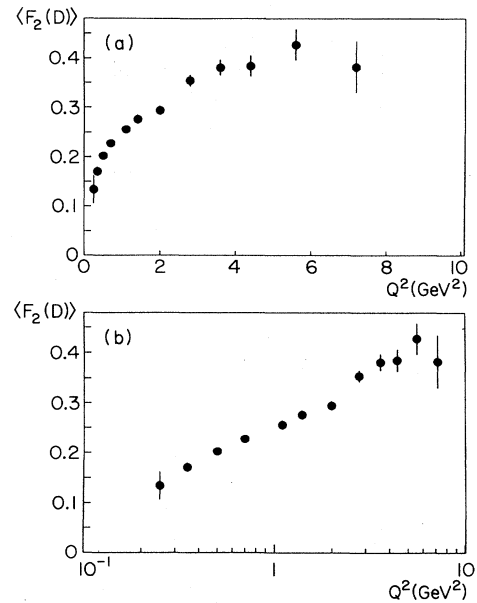


FIG. 30. Mean value of $F_2(D)$ for $x < 0.1$ as a function of Q^2 , obtained by EMC NA28 on (a) linear and (b) logarithmic scales in Q^2 . Error bars represent statistical and systematic errors summed in quadrature (from Arneodo *et al.*, 1990, 1988).

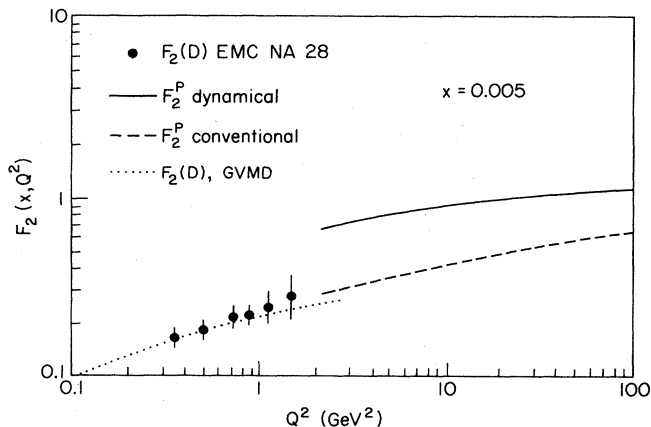


FIG. 31. $F_2(D)$ as a function of Q^2 at $x=0.005$, from EMC NA28, compared to the proton structure function F_2^p predicted from the dynamical (Glück *et al.*, 1988, 1989) and conventional (Diemoz *et al.*, 1988) parton distributions and to $F_2(D)$ from the GVMD calculations (Kwieciński and Badelek, 1989). Error bars represent statistical and systematic errors summed in quadrature (from Arneodo *et al.*, 1990, 1988).

(see Fig. 31). The comparison improves, however, in the new version of the dynamical structure-function calculations (Fig. 32), when valencelike gluons are included at the low scale (Glück *et al.*, 1990, 1991).

Recently NMC presented preliminary results on low- x measurements of $F_2(H)$ and $F_2(D)$ (Bird *et al.*, 1991), Figs. 33–35, obtained assuming $R(x, Q^2)$ given by the parametrization of the SLAC results (Whitlow, 1990; Whitlow *et al.*, 1990; Bodek *et al.*, 1991). These are the first precise data on $F_2(H)$ in this region of x ; a significant statistical improvement was also obtained over the EMC NA28 measurements of $F_2(D)$. The two experiments agree well within errors.

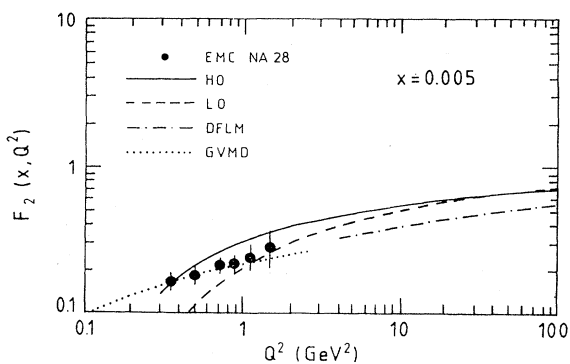


FIG. 32. $F_2(D)$ as a function of Q^2 at $x=0.005$, from EMC NA28, compared to the proton structure function F_2^p predicted from the modified dynamical calculations in higher order (solid curve) and leading order (dashed curve) of Glück *et al.* (1990, 1991), the conventional calculation (dot-dash curve) of Diemoz *et al.* (1988), and to $F_2(D)$ from the GVMD calculations of Kwieciński and Badelek (1989). From Glück *et al.* (1990, 1991).

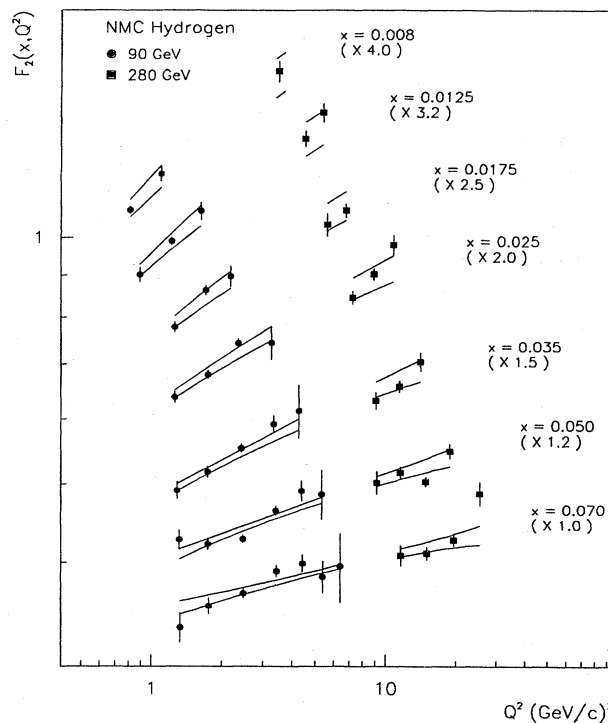


FIG. 33. Proton structure function $F_2(H)$ from the preliminary analysis of the NMC data taken at two energies of the muon beam. Error bars are statistical, systematic error bands are plotted around fitted function. In addition there is an overall normalization error of 4% (from Bird *et al.*, 1991).

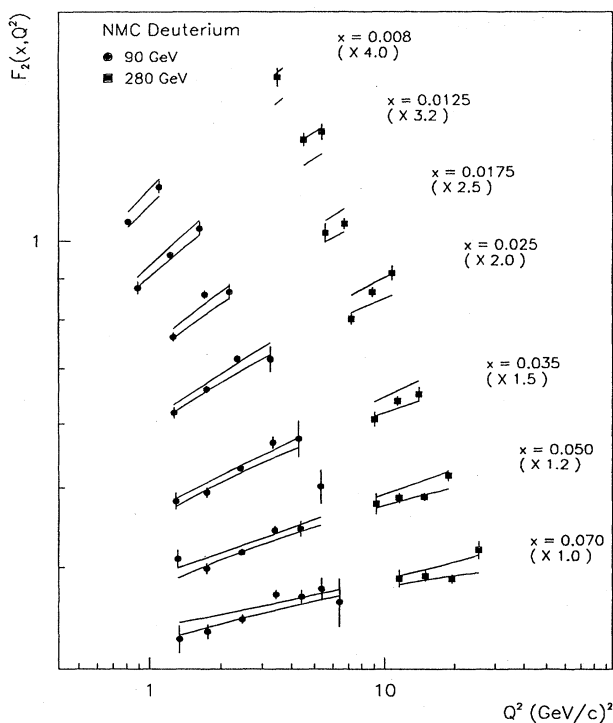


FIG. 34. As in Fig. 33, but plotted is the nucleon structure function $F_2(D)$ (from Bird *et al.*, 1991).

3. Nucleon structure function from heavy nuclei

The nucleon structure function obtained from calcium, $F_2(\text{Ca})$, is shown in Figs. 36 and 37 as a function of x and Q^2 (Arneodo *et al.*, 1990, 1988). These figures also include data from the EMC NA2 muon-iron experiment (Aubert *et al.*, 1986) and the CDHSW neutrino-iron results (Berge *et al.*, 1991), both obtained with $R = 0$. The charged-lepton structure function was computed from the CDHSW ν and $\bar{\nu}$ data, neglecting the contribution of charm but making a correction for the strange quark distribution (Berge *et al.*, 1991). Within errors there is reasonable agreement between the different experiments, except perhaps in the $x = 0.015$ bin, where the CDHSW data appear to be somewhat higher than the NA28 data. Unlike the deuterium results (Fig. 26), Fig. 36 shows that F_2 from calcium tends to decrease with x , indicating the onset of shadowing. There is no such trend in the neutrino data, which are, however, rather sparse in the appropriate low- x region. Figure 37 shows that in the calcium data a similar $\log Q^2$ dependence exists to that observed for deuterium (Fig. 27). Numerical values of the $F_2(\text{Ca})$ and $F_2(\text{C})$, as well as the coefficients of the function fitted to the data, can be found in Arneodo *et al.* (1990, 1988).

In Figs. 38–41, the new, precise CCFR neutrino-iron (preliminary) results are shown, together with the similar CDHSW data and the SLAC and BCDMS results on deuterium (Mishra *et al.*, 1991). There is a remarkable shape disagreement between CCFR and CDHSW mea-

surements at $x < 0.225$. However, the latter experiment has large systematic errors at low x , which are not marked on the figures. Moreover the compared sets of data were obtained with different functional shapes of $R(x, Q^2)$: the parametrization from the SLAC measurements (Whitlow, 1990; Whitlow *et al.*, 1990; Bodek *et al.*, 1991) was used for the CCFR, while $R = 0$ was used for the CDHSW data. Further, a correction for the charm production threshold was applied only for the CCFR data. Therefore the low- x disagreement between the two neutrino experiments may not be as serious as the above comparison would imply.

The recent CCFR measurements permitted a check on the Gross-Llewellyn Smith sum rule, S_{GLS} , defined as

$$S_{\text{GLS}} = \int_0^1 \frac{x F_3}{x} dx \approx 3 \left[1 - \frac{\alpha_s(Q^2)}{\pi} \right]. \quad (40)$$

Theoretically, taking $\Lambda_{\overline{\text{MS}}} = 250$ MeV, $S_{\text{GLS}} = 2.63$. The result for $0.005 < x < 0.85$ and at $\langle Q^2 \rangle = 3$ GeV² is $S_{\text{GLS}} = 2.50 \pm 0.018(\text{stat}) \pm 0.078(\text{syst})$ (Shaevitz, 1992), i.e., the sum rule is satisfied at the 2σ level.

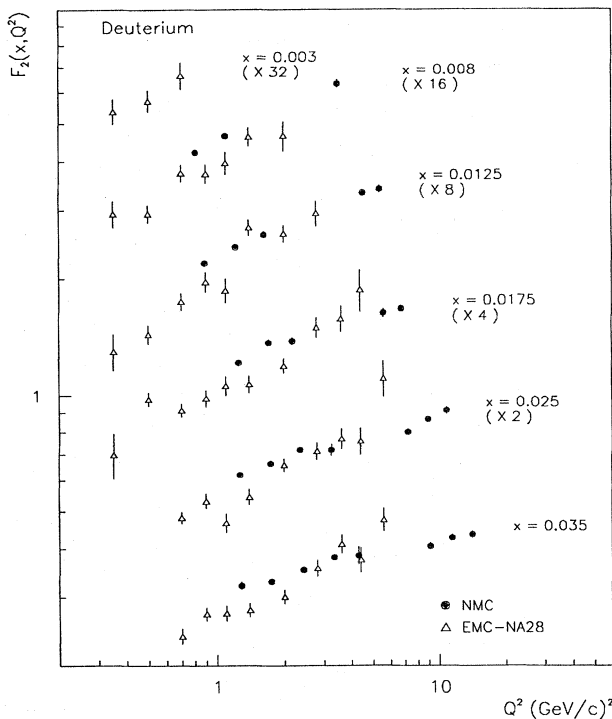


FIG. 35. Same data as in Fig. 34 compared to the results of the EMC NA28. Errors are statistical (from Bird *et al.*, 1991).

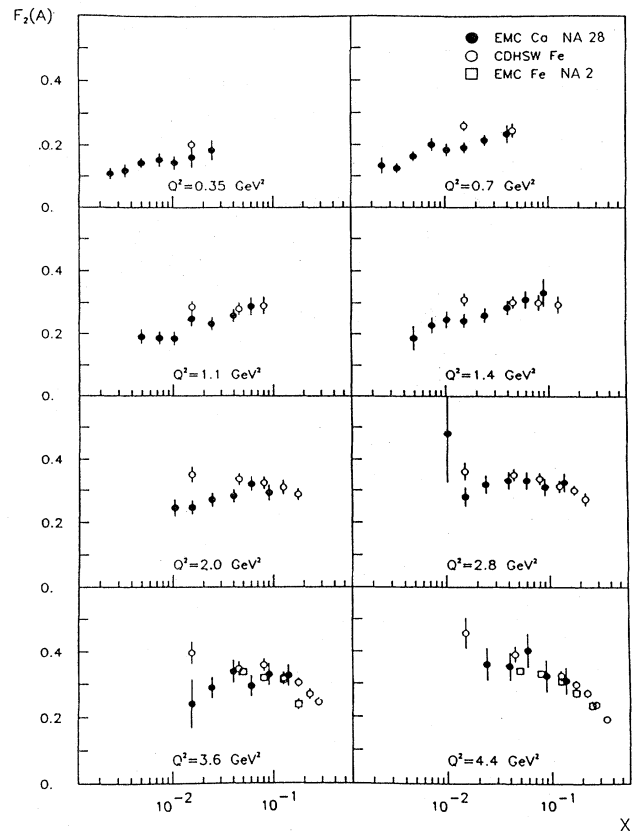


FIG. 36. Nucleon structure function $F_2(\text{Ca})$ obtained from calcium as a function of x for different intervals of Q^2 , from EMC NA28, compared to the results of CDHSW (Berge *et al.*, 1991) and EMC (Aubert *et al.*, 1986), both obtained with iron and evaluated with $R = 0$. Error bars represent statistical and systematic errors summed in quadrature. In addition there is an overall normalization error of 8% (from Arneodo *et al.*, 1990, 1988).

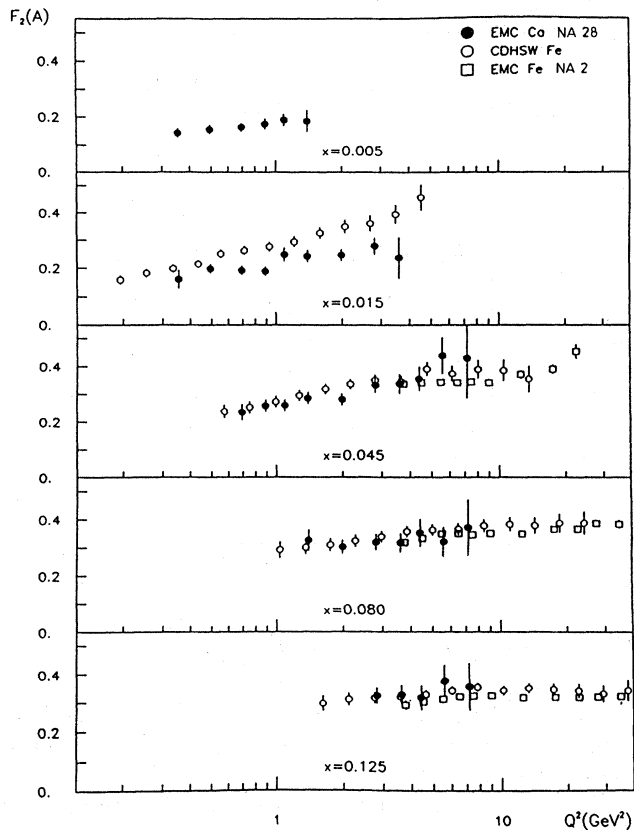


FIG. 37. $F_2(\text{Ca})$ as a function of Q^2 for different intervals of x . Errors as in Fig. 36 (from Arneodo *et al.*, 1990, 1988).

4. Structure-function ratios

a. $F_2(D)/F_2(H)$

The x dependence of the $F_2(D)/F_2(H)$ ratio has been determined by the NMC with high statistical and systematic accuracy (Allasia *et al.*, 1990; Amaudruz *et al.*, 1991a, 1992a; Brüll *et al.*, 1991). At low x both statistical and systematic errors are below 2%. These are practically the only data for $x < 0.06$. Accurate measurements of this ratio put strong constraints on parton distributions derived from analyses of deep-inelastic scattering, prompt photon, and leptonproduction data (Harriman *et al.*, 1990). The NMC determined the ratio $r = F_2^D/F_2^H = \sigma(\mu D)/\sigma(\mu H) - 1$, where the ratio $\sigma(\mu D)/\sigma(\mu H)$ was the measured quantity. The results, shown in Fig. 42, extend down to $x = 0.003$; the average Q^2 for the lowest x value is 0.6 GeV^2 and $r = 0.990 \pm 0.016(\text{stat}) \pm 0.026(\text{syst})$ (Brüll *et al.*, 1991; Amaudruz *et al.*, 1992a). The interesting quantity, $R = F_2(D)/F_2(H) = (r + 1)/2$, is then $0.995 \pm 0.008 \pm 0.013$ at $x = 0.003$. The measured ratio r decreases monotonically with increasing x . Thus within errors there is no evidence for virtual-photon shadowing in the deuteron for $x > 0.003$. Indeed, the effect is expected to be small due to the weak deuteron binding. There is, however, an indication of shadowing of low-energy real ($Q^2 = 0$) photons on the deuteron. The ratio of the total photoproduction cross section $\sigma_{\text{tot}}(\gamma D)/2\sigma_{\text{tot}}(\gamma H)$ is around 0.95 at the photon energy $\nu \sim 18 \text{ GeV}$ (Alekhin *et al.*, 1987). No data exist for $\sigma_{\text{tot}}(\gamma D)$ at $\nu > 18 \text{ GeV}$.

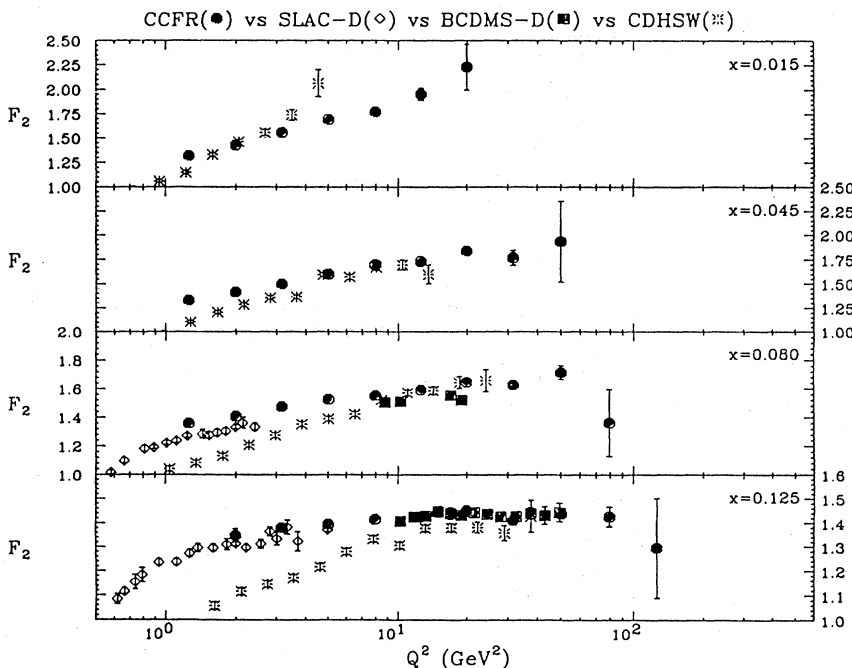


FIG. 38. Nucleon structure function $F_2(\text{Fe})$ from the preliminary analysis of the CCFR data compared to the $F_2(\text{Fe})$ of CDHSW, $F_2(D)$ of SLAC, and $F_2(D)$ of BCDMS. Comparison with deuterium data was made after correcting for the EMC effect in iron. Errors are statistical. From Mishra *et al.* (1991).

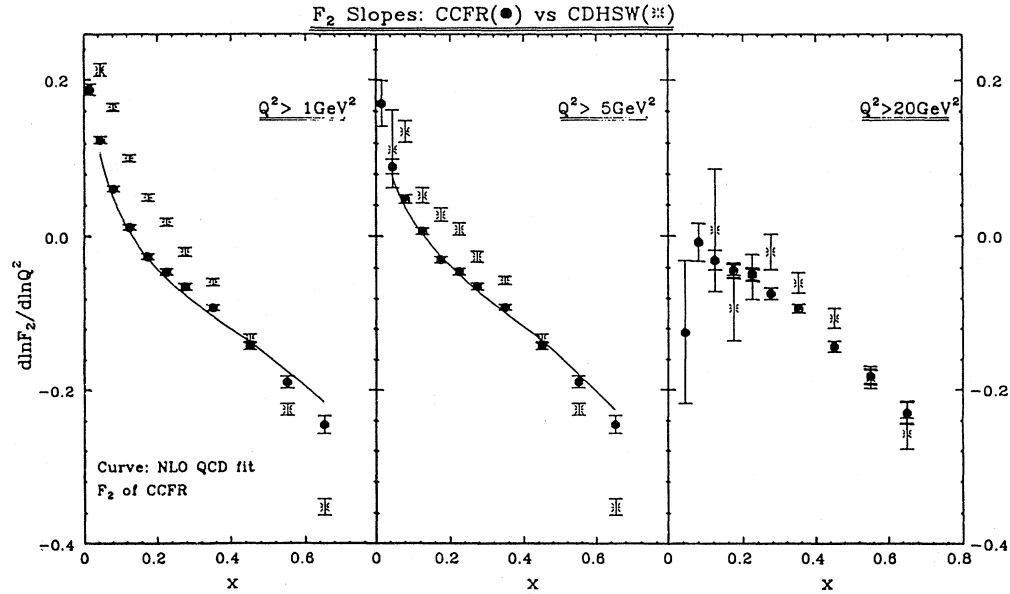


FIG. 39. Slopes of the Q^2 dependence of $F_2(\text{Fe})$ for the preliminary CCFR data (from Mishra *et al.*, 1991).

A calculation of the virtual-photon shadowing in the deuteron based on the double-interaction formalism, in which shadowing was related to inclusive diffractive processes, was carried out for the Q^2 range covered by the NMC results (Zoller, 1992a, 1992b; Badełek and Kwieciński, 1992). Badełek and Kwieciński (1992) considered both the vector-meson and the parton contributions to shadowing for low and high Q^2 values, including QCD corrections with parton recombination for high Q^2 . As expected, the shadowing effects were found to be

small, i.e., less than 2% or so. The data can accommodate this, but they do not exclude the complete lack of shadowing.

The NMC measurements allow a check to be made on the Gottfried sum rule S_G , defined as

$$S_G \equiv \int_0^1 \frac{dx}{x} (F_2^p - F_2^n). \quad (41)$$

Separating the quark distributions into valence and sea components, and assuming proton-neutron isospin sym-

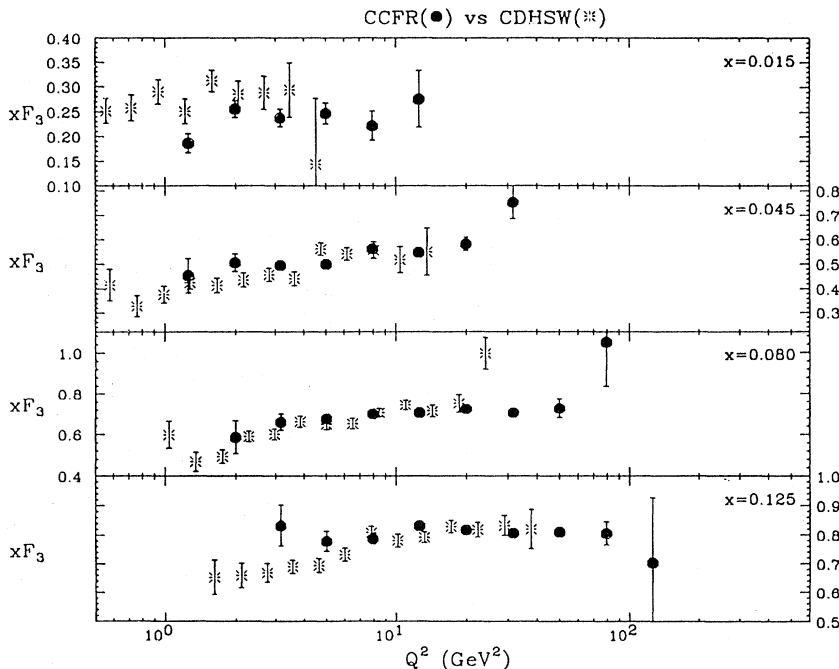


FIG. 40. As in Fig. 38 but plotted is the $xF_3(\text{Fe})$ (from Mishra *et al.*, 1991).

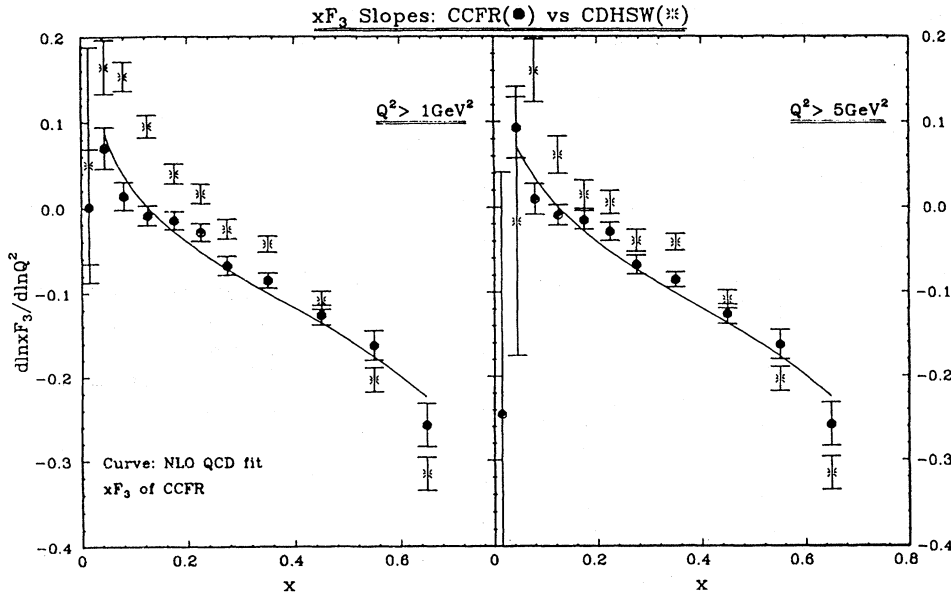


FIG. 41. As in Fig. 39 but for $x F_3(\text{Fe})$ (from Mishra *et al.*, 1991).

metry, one obtains

$$S_G = \frac{1}{3} + \frac{2}{3} \int_0^1 [\bar{u}(x) - \bar{d}(x)] dx, \quad (42)$$

where $\bar{u} \equiv \bar{u}_p = \bar{d}_n$ and $\bar{d} \equiv \bar{d}_p = \bar{u}_n$ are the distributions of the sea quarks (heavier flavors are neglected). For a flavor-symmetric sea, $\bar{d} = \bar{u}$, the second term vanishes and the expected result is $S_G = \frac{1}{3}$. The NMC data determine S_G for $0.004 < x < 0.8$ through the relation

$$F_2^p - F_2^n = 2F_2(D) \frac{1 - F_2^n/F_2^p}{1 + F_2^n/F_2^p}. \quad (43)$$

For the region $x < 0.004$, an extrapolation was used and $F_2(D)$ was obtained from a fit to all available electron and muon scattering data. The value of the Gottfried sum rule in the measured region at $Q^2 = 4 \text{ GeV}^2$ is $S_G(0.004 - 0.8) = 0.227 \pm 0.007(\text{stat}) \pm 0.014(\text{syst})$. Summing the contributions from the measured and unmeasured regions and adding the errors quadratically, Amaudruz *et al.* (1991a) obtained the value $S_G = 0.240 \pm 0.016$. The error accounts also for the low- x extrapolation uncertainties. Any Q^2 dependence was neglected. The result is significantly below the simple quark-parton model prediction of $\frac{1}{3}$. While a flavor-asymmetric sea appears to be a likely explanation, other effects should also be considered (see Kumano and Londergan, 1990, for a review of the literature). It is possible to make parametrizations of parton distributions that agree with the NMC measurements of r and are constrained to fulfill the Gottfried sum rule (Martin *et al.*, 1990). With these parametrizations, one-third of the Gottfried sum comes from the region $x < 0.004$. This, however, seems unlikely given the CCFR results on the Gross-Llewellyn Smith sum rule for iron (see Sec. III.C.3).

The Q^2 variation of the F_2^n/F_2^p ratio has been studied by Brüll *et al.* (1991) and Amaudruz *et al.* (1992a). For each x bin they parametrized the ratio as a linear function of $\log(Q^2)$. The slopes obtained in this way are shown in Fig. 43. No Q^2 dependence of F_2^n/F_2^p is observed for $x < 0.1$.

b. $F_2(A)/F_2(D)$

Comparison of the structure functions from nuclear and elementary targets allows a study of the influence of

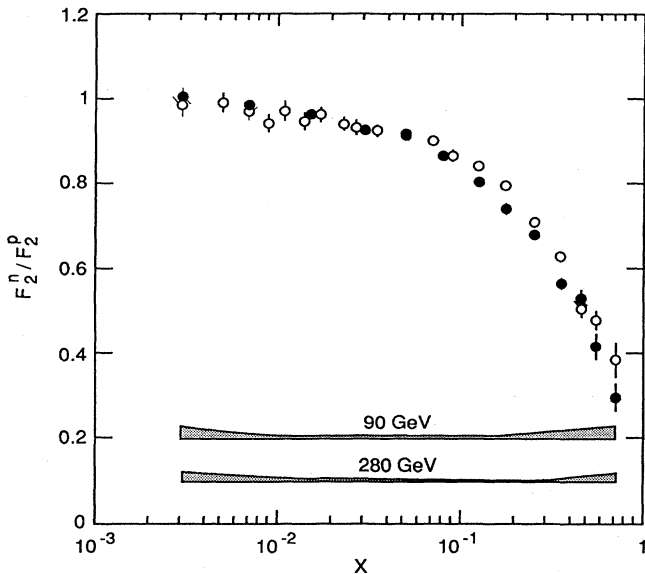


FIG. 42. The ratio $r = F_2^n/F_2^p = \sigma(\mu D)/\sigma(\mu H) - 1$ as a function of x , measured at 90- and 280-GeV incident muon energy by the NMC. The average Q^2 changes from point to point and is different for the two data sets. The bands show the systematic uncertainties (from Brüll *et al.*, 1991, and Amaudruz *et al.*, 1992a).

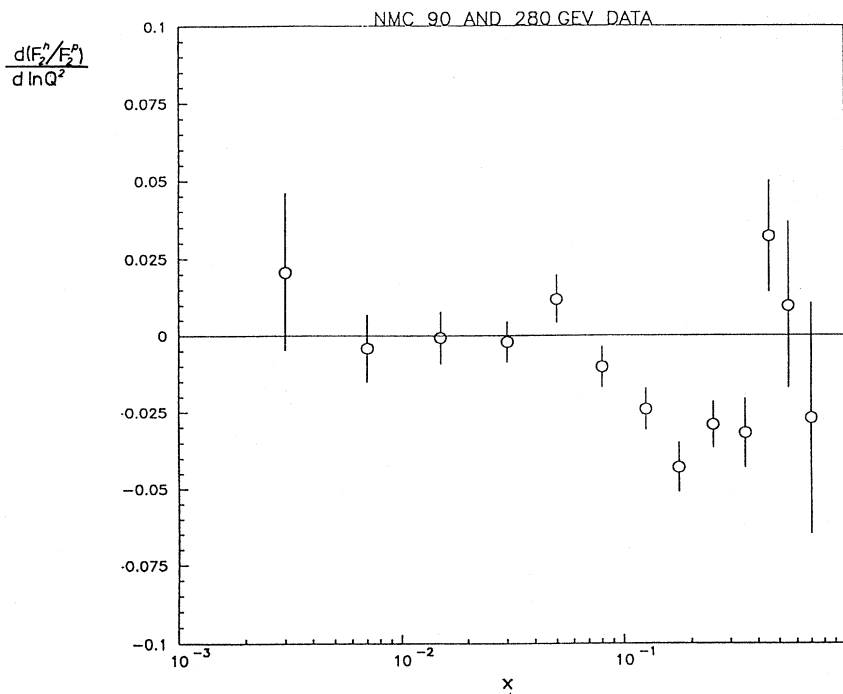


FIG. 43. $d(F_2^n/F_2^p)/d \ln(Q^2)$ as a function of x (from Brüll *et al.*, 1991, and Amaudruz *et al.*, 1992a). Error bars represent statistical and systematic errors summed in quadrature.

the nuclear medium. Deuterium is traditionally taken as a free-nucleon target in the comparisons (Arnold *et al.*, 1984; Bari *et al.*, 1985; Ashman *et al.*, 1988; Arneodo *et al.*, 1990, 1988; Amaudruz *et al.*, 1991b). The small amount of shadowing predicted for the deuteron (Badežek and Kwieciński, 1992) justifies this procedure up to almost 2% accuracy at $x \sim 0.004$.

Figure 44 shows the x dependence of the structure-function ratios $F_2(A)/F_2(D)$ obtained on $A=4$, $\langle A \rangle=12$, and $A=40$ targets in the charged-lepton scattering experiments: SLAC (Arnold *et al.*, 1984), BCDMS (Bari *et al.*, 1985), EMC (Ashman *et al.*, 1988; Arneodo *et al.*, 1990, 1988), and NMC (Amaudruz *et al.*, 1991b). The data extrapolate smoothly to those obtained with real photons of $\nu=100$ GeV where $\sigma_{\text{tot}}(\gamma\text{Cu})/64\sigma_{\text{tot}}(\gamma\text{H})$ is about 0.7 (Caldwell *et al.*, 1979) and join to those obtained with electrons and muons at larger x . The data show a pronounced signal of shadowing, which increases with nuclear atomic number. For $A=40$ targets, shadowing does not show any flattening, even at the lowest values of x ($x \sim 0.003$). This may not be the case for the E665 results, in which the preliminary measurements on the ^{131}Xe nucleus show that, in the x range 0.0002 to 0.002, the $F_2(\text{Xe})/F_2(D)$ ratio remains roughly constant at ~ 0.70 (Fig. 45; Jaffe *et al.*, 1991; Schellman *et al.*, 1991). The intermediate x enhancement ("antishadowing") is clearly manifested in the data of Fig. 44 for x between 0.1 and 0.3. The crossover point between shadowing and antishadowing shifts towards larger values of x when A increases. Figure 46 shows the x dependence of the slopes from a linear fit in $\ln Q^2$ of the $F_2(A)/F_2(D)$ ratio for the NMC. No clear Q^2 depen-

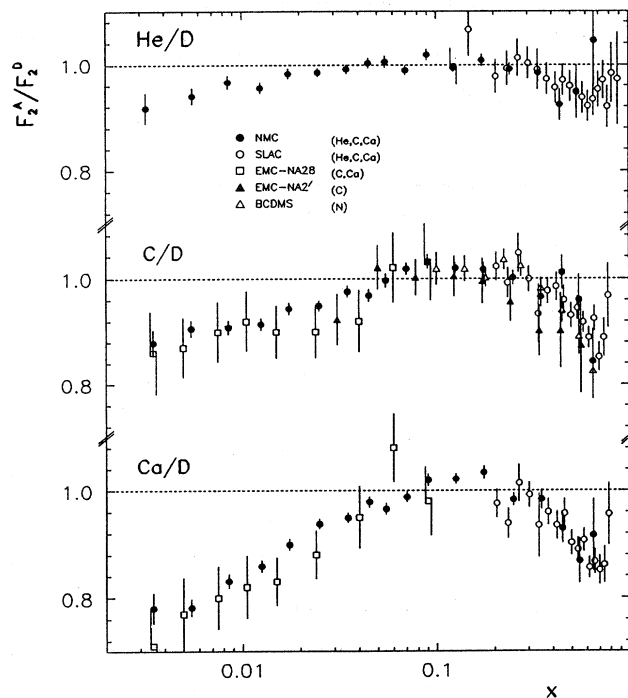


FIG. 44. Structure-function ratios $F_2(A)/F_2(D)$ as functions of x averaged over Q^2 , obtained by NMC, compared to the results of SLAC E139 (Arnold *et al.*, 1984), EMC NA2 (Ashman *et al.*, 1988), and EMC NA28 (Arneodo *et al.*, 1990, 1988). Also shown are the data $F_2(N)/F_2(D)$ from BCDMS (Bari *et al.*, 1985). Error bars represent statistical and systematic errors summed in quadrature (from Amaudruz *et al.*, 1991b).

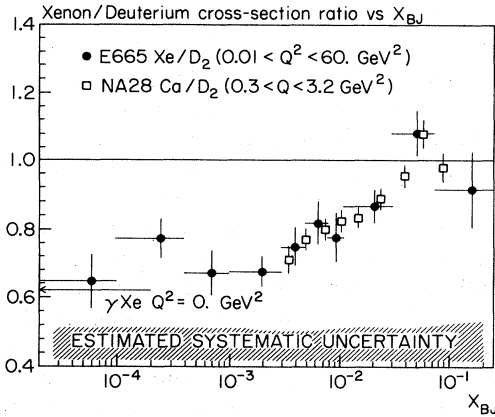


FIG. 45. Preliminary results of the E665 experiment on the $\sigma(\text{Xe})/\sigma(\text{D})$ ratio compared to the EMC NA28 points (Arneodo *et al.*, 1990, 1988). The band shows the estimated systematic uncertainty (from Jaffe *et al.*, 1991, and Schellman *et al.*, 1991).

dence is observed in the fixed x intervals, which also implies a lack of strong ν dependence in these intervals. This suggests that the vector-meson-dominance model, at least in its simplest form, is not the main explanation for the shadowing observed in the data, or, in other words, shadowing is a leading-twist phenomenon.

The sensitivity of the nuclear cross section to nuclear size and density was investigated in the NMC measurements of the $F_2(\text{C})/F_2(\text{Li})$ and $F_2(\text{Ca})/F_2(\text{Li})$ ratios (Amaudruz *et al.*, 1992b). ${}^6\text{Li}$ and ${}^{12}\text{C}$ nuclei were found

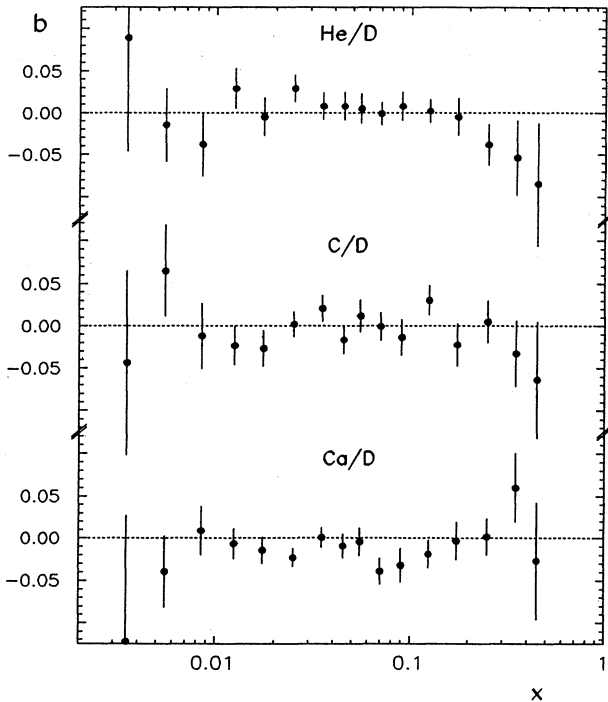


FIG. 46. The slopes b from a linear fit $\ln Q^2$ of the $F_2(A)/F_2(D)$ ratio for each x bin separately up to $x = 0.45$, obtained by NMC. The errors shown are statistical only (from Amaudruz *et al.*, 1991b).

to have approximately equal radii (2.6 and 2.5 fm, respectively), but their mean densities differ by a factor of 2 (0.04 and 0.09 fm^{-3}), while ${}^{40}\text{Ca}$ has a mean density (0.11 fm^{-3}) comparable to that of ${}^{12}\text{C}$ but a much larger radius (3.5 fm). The results, Fig. 47, show that the shadowing depends on both parameters, while the “antishadowing” signal appears to be primarily dependent on the target density.

IV. PROBING THE SMALL- x REGION AT HERA

The forthcoming ZEUS and H1 experiments at the HERA ep collider will provide the first test of the

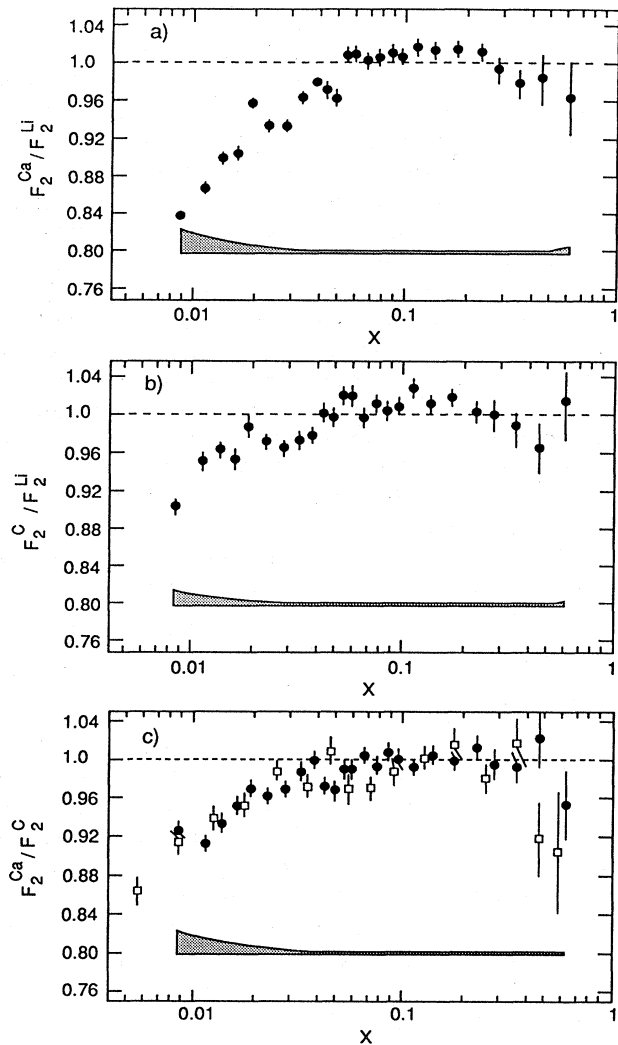


FIG. 47. Structure-function ratios $F_2(A_1)/F_2(A_2)$ as functions of x averaged over Q^2 , obtained by the NMC at 90-GeV incident muon momentum (from Amaudruz *et al.*, 1992b). Errors are statistical; the bands show the systematic uncertainties. The normalization uncertainties (not included in the errors) are 0.8%, 0.7%, and 0.5% for Ca/Li, C/Li, and Ca/C structure-function ratios. The open symbols in (c) were obtained by dividing the Ca/D and C/D structure function ratios from the NMC measurements at 200 GeV (Amaudruz *et al.*, 1991b).

theoretical ideas behind small- x physics. In this section we shall briefly review the quantities that are sensitive to small- x phenomena. More systematic and detailed investigations are being performed by the HERA working groups.

One of the main subjects to be studied by the experiments at HERA will be the proton structure function and parton distributions in the new kinematic region. A precise measurement of the F_2 structure function will be possible for (Feltesse, 1988)

$$\begin{aligned} 5 \times 10^{-5} \leq x \leq 0.6, \\ Q^2 \geq 5 \text{ GeV}^2, \\ y \geq 0.1, \end{aligned} \tag{44}$$

assuming a center-of-mass energy $\sqrt{s} = 314 \text{ GeV}$. This should be compared with the range of x explored so far in lepton-nucleon scattering at similar values of Q^2 : $0.03 < x < 0.9$. Thus the x range can be extended by more than two orders of magnitude. A large number of events (small statistical errors) is expected for F_2 in the small- x region, $x < 0.01$ corresponding to $Q^2 < 100 \text{ GeV}^2$ at HERA (Wolf, 1990).

To illustrate the different approaches used so far in the description of the small- x region, let us recall the basic assumptions of the three recent parametrizations of the parton distribution functions for the proton (see also Sec. II.D.4). All of them are based on next-to-leading-order analyses and take into account recent muon and neutrino deep-inelastic data (EMC, CDHSW, BCDMS, and NMC; Aubert *et al.*, 1987; Benvenuti *et al.*, 1989; Allasia *et al.*, 1990; Berge *et al.*, 1991).

In the analysis by Morfin and Tung (1991), the following form of the parton distribution in the proton was assumed:

$$xf^a(x, Q^2) \sim x^{A_1^a} (1-x)^{A_2^a} \ln^{A_3^a} \left[1 + \frac{1}{x} \right], \tag{45}$$

where a runs over the flavors. Their treatment of the small- x region differed from other analyses (Charchuła *et al.*, 1990; Abramowicz *et al.*, 1991a) on two essential points: (i) the parameter A_1 of the gluon and sea-quark distributions was a free parameter in the data analysis, i.e., its value at $Q_0^2 = 4 \text{ GeV}^2$ was determined by the data rather than by some arbitrary assumption; (ii) the factor $\ln^{A_3}(1+1/x)$, in addition to the traditional power-law form, allowed for a logarithmic extrapolation to the small- x region.

With additional assumptions (choice of the fitting parameters, symmetry of the sea quarks, choice of the data) these authors obtained several sets of parton distributions that reproduce the data very well but lead to different predictions beyond the presently measured region. For example, the input gluon distribution at $Q_0^2 = 4 \text{ GeV}^2$ in the sets "B1" and "B2" (which are both based on the $\overline{\text{MS}}$ data) has the following small- x behavior (in the $\overline{\text{MS}}$ scheme): (i) $xG(x, Q_0^2) \sim x^{-0.07}$ ("B1" set), (ii)

$xG(x, Q_0^2) \sim x^{-0.59}$ ("B2" set).

The approach of Kwieciński, Martin, Roberts, and Stirling (Kwieciński *et al.*, 1990) relied on assumptions based on Regge theory. Shadowing corrections were included here by modifying the initial distributions (at Q_0^2) in the region of $x < x_0 = 10^{-2}$ and by including nonlinear terms in the evolution equation. In addition, two different scenarios for shadowing phenomena were considered. In the first, saturation of partons appeared over the full transverse size of the nucleon (radius $R \sim 5 \text{ GeV}^{-1}$). The second prescription assumed that saturation begins in a nonuniform fashion, namely, in smaller regions of size $R \sim 2 \text{ GeV}^{-1}$. This is the so-called "hot spots" picture (Mueller, 1990b). The resulting parametrization consists of several sets of individual parton distributions, with the following assumptions about gluon behavior at small x : (i) $xG(x, Q_0^2) \sim x^{0.5}$ ("B-" set); (ii) $xG(x, Q_0^2) \sim x^{-0.5}$ with shadowing corrections in two different scenarios, ("B-5" and "B-2" sets); (iii) $xG(x, Q_0^2) \sim x^0$ ("B0" set).

Finally, in the approach of Glück, Reya, and Vogt (1990, 1991), radiatively generated gluon and sea-quark densities were parametrized in the form

$$\begin{aligned} xf^a(x, Q^2) = [x^a (A + Bx + Cx^2) (\ln 1/x)^b \\ + s^a \exp(-E + \sqrt{E's\beta \ln 1/x})] (1-x)^D, \end{aligned} \tag{46}$$

where $s = \ln[\ln(Q^2/\mu_0^2)/\ln(\mu_{\text{HO}}^2/\mu_0^2)]$, μ_0, μ_{HO} are around 0.3 GeV and $a = G, \bar{u}, \bar{d}$. The quantities A, B, C , etc. are second-order polynomials of s .

In Fig. 48 we present gluon distributions calculated

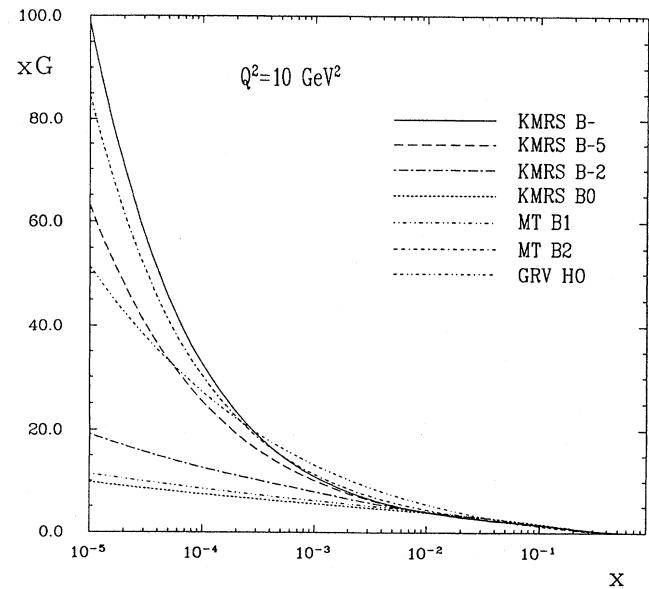


FIG. 48. Behavior of the gluon distribution function $xG(x, Q^2)$ at $Q^2 = 10 \text{ GeV}^2$, as predicted by parametrizations of Glück, Reya, and Vogt (1990, 1991), Kwieciński *et al.* (1990), and Morfin and Tung (1991).

from the above parametrizations at $Q^2=10 \text{ GeV}^2$ (next-to-leading-order parton distributions, $\overline{\text{MS}}$ scheme). In Figs. 49 and 50 the respective behavior of F_2 and F_L structure functions for the proton is shown. Note that available parametrizations of parton distribution functions, especially those using recent data in the fitting procedure, reproduce the experimentally measured F_2 well for $x > 0.01$ (Abramowicz *et al.*, 1991a). However, their predictions at smaller x diverge. The predictions of the parametrizations for the structure function F_2^p down to $x = 10^{-5}$ are shown at $Q^2=10 \text{ GeV}^2$ in Fig. 49(a). The spread between different curves is substantial in the HERA region. For completeness the predictions for F_2^p

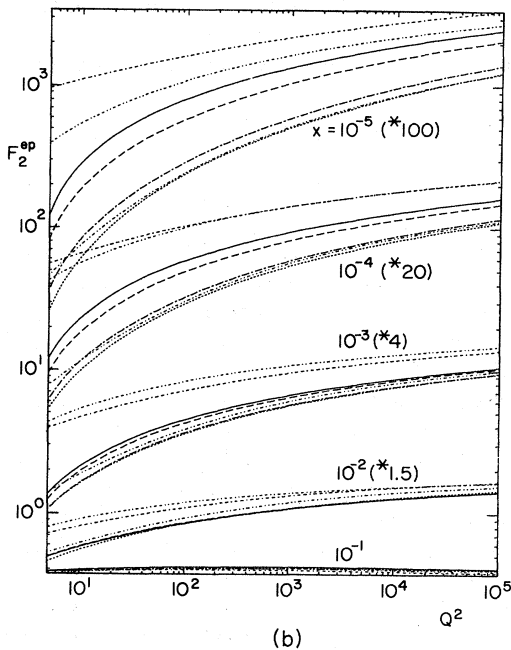
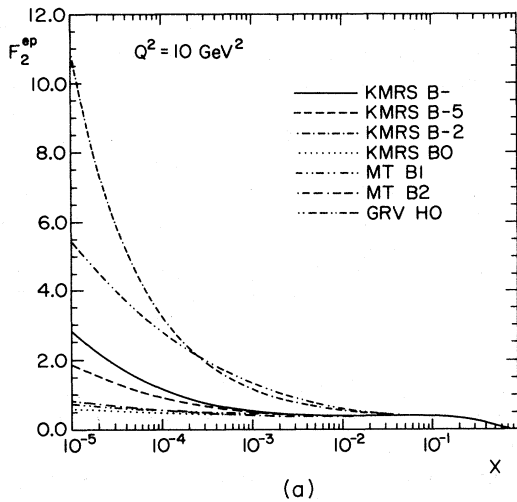


FIG. 49. Predictions for $F_2^p(x, Q^2)$ according to parametrizations of Glück, Reya, and Vogt (1990, 1991), Kwieciński *et al.* (1990), and Morfin and Tung (1991): (a) as a function of x at $Q^2=10 \text{ GeV}^2$; (b) as a function of Q^2 for several x values.

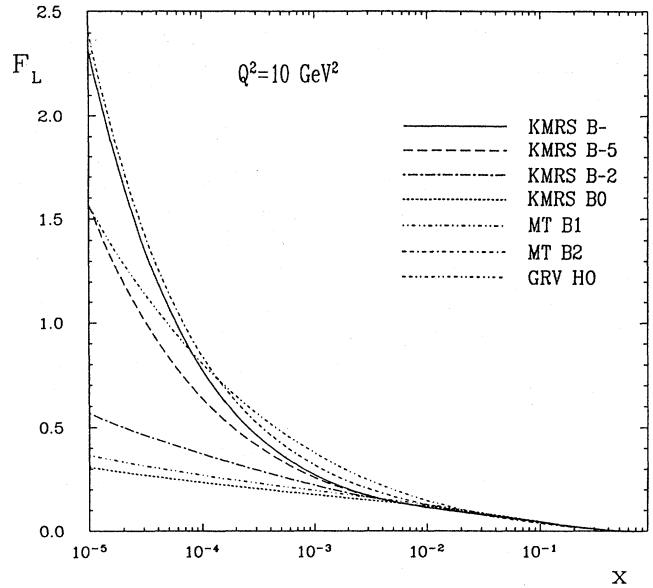


FIG. 50. Predictions for $F_L(x, Q^2)$ at $Q^2=10 \text{ GeV}^2$, according to the parametrizations of Glück, Reya, and Vogt (1990, 1991), Kwieciński *et al.* (1990), and Morfin and Tung (1991).

as a function of Q^2 for various x are presented in Fig. 49(b). The spread of the predictions increases as x decreases. It appears to be constant with Q^2 . The differences in Fig. 49 come mainly from assumptions about the x behavior of parton distributions at the input Q_0^2 scale, as discussed in Sec. II.D.4. For the same input distribution, shadowing corrections can also change the small- x behavior of F_2 (compare predictions of the “B-” set with those of the “B-5” and “B-2” sets). Because of the large number of events expected at small x , there is hope of differentiating experimentally between various predictions if the systematic effects can be kept below 3%.

In spite of the large differences between the various predictions, it might be quite difficult to observe new phenomena beyond any doubt. For example, a measurement of a flat structure function may arise both from a “conventional” parton distributions of “B0” and from a $1/\sqrt{x}$ type behavior with strong shadowing effects (“B-2” set). Even the Q^2 evolution, which differentiates between solutions of linear and nonlinear equations, may not be helpful in this case.

As a remedy for these kinds of difficulties two experiments specifically designed to look for signals of new phenomena at small x were proposed. Both of them refer to the “hot spots” picture mentioned in Sec. II.D.3. Essentially one should look at exclusive final states, in a specific region of phase space, which measure the parton distribution inside a limited region of the proton. In the proposal of Mueller (1990b) one would measure a one-jet inclusive cross section in the region of $Q^2 \geq k_{\text{Ljet}}^2 \gg Q_0^2$ and $x_{\text{jet}} \gg x$, where k_{Ljet}^2 is the transverse momentum of a measured jet and x_{jet} denotes the longitudinal momentum fraction carried by this jet. The proposal of Ryskin

(1988, 1990) is based on the hypothesis that in the diffractive dissociation of the photon the saturation effect substantially changes the value of the differential cross section.

As the small- x region is highly populated by gluons, several methods have been proposed for extraction of the gluon distribution in this region. The conventional one is by QCD analysis of the F_2 structure function, as the gluon distribution affects its Q^2 evolution. There are, however, several drawbacks to this method, such as the restricted Q^2 range at fixed x , the requirement of simultaneously fitting $xG(x, Q^2)$ and Λ , the type of evolution equation to be used (linear or nonlinear, in what range of x), etc. The determination of the gluon distribution from the F_L structure function seems to lead to a higher precision. At low x , F_L is almost directly related to the gluon distribution (see, for example, Cooper-Sarkar *et al.*, 1988):

$$xG(x, Q^2) \sim \frac{3}{5} 5.9 \left[\frac{3\pi}{4\alpha_s(Q^2)} F_L(0.4x, Q^2) - \frac{1}{2} F_2(0.8x, Q^2) \right] \quad (47)$$

and reflects the small- x behavior of gluons very clearly, as can be seen by comparing Fig. 48 (gluon distribution) with Fig. 50 (F_L distribution). HERA offers the possibility of determining F_L at x values of the order of 10^{-3} and Q^2 values of the order of 10–100 GeV^2 , through measurements at at least two different proton-beam energies, (see Sec. III.B). Other methods of determining the gluon distribution at small x rely on J/Ψ production (Tkaczyk *et al.*, 1988) and open heavy-flavor production (Barbagli and D'Agostini, 1988; D'Agostini and Mondaldi, 1990; Abraham *et al.*, 1991).

In the context of probing the low- x region it should also be mentioned that HERA will be able to investigate the Pomeron structure through diffractive deep-inelastic scattering (Donnachie and Landshoff, 1984, 1987; Ingelman and Schlein, 1985; Berger *et al.*, 1987; Ryskin, 1988, 1990; Streng, 1988; Bartels and Ingelman, 1990; Ingelman, 1990; see Sec. II.E). It may be possible, for example, to separate the gluon and the quark (if any) content of the Pomeron, since they lead to different processes.

Finally we shall mention the low- x QCD predictions for nuclear targets using the deuteron as an example. For large Q^2 , the shadowing contribution to the deuteron structure function is related to the shadowing terms in the quark and antiquark distributions in the deuteron. The shadowing terms are also present in the gluon distribution. At $x \leq 10^{-4}$, two perturbative QCD corrections to shadowing become important: the logarithmic scaling violations induced by QCD evolution and possible recombination of partons from different nucleons in the deuteron (see Fig. 13), giving additional terms in the evolution equations. The corrections are displayed in Fig. 51 and compared with shadowing obtained without the QCD evolution and parton recombination (Badełek and

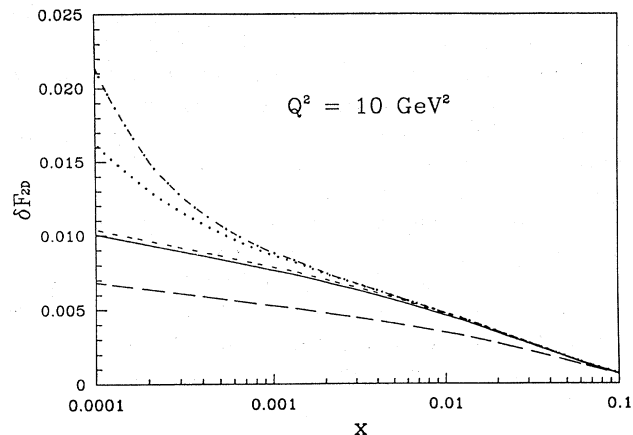


FIG. 51. Effects of QCD evolution on the shadowing contribution to the deuteron structure function $\delta F_2(D)$, for $Q^2=10 \text{ GeV}^2$: long-dashed curve, unevolved δF_2 ; solid curve, QCD evolution starting from $Q_0^2=4 \text{ GeV}^2$ without parton recombination. The remaining three curves show effects of the QCD evolution with recombination included and correspond to three different gluon distributions in a nucleon: short-dashed curve, results for $xG(x, Q^2) \rightarrow \text{const}$ for $x \rightarrow 0$; dotted curve, results for the gluon distribution containing both the singular $1/\sqrt{x}$ behavior and shadowing effects; dashed-dotted line, results for $xG(x, Q_0^2) \rightarrow 1/\sqrt{x}$. From Badełek and Kwieciński (1992).

Kwieciński, 1992). Both effects change substantially the low- x results, the parton recombination mechanisms being very sensitive to gluon distributions in the nucleon. The deuteron structure function itself is also very sensitive to the gluon distribution in that region (see the discussion above), and therefore the shadowing turns out to be again only a 2% effect, almost independent of the assumed small- x behavior of the parton distributions.

V. SUMMARY AND OUTLOOK

In this report we have reviewed the present understanding of the deep-inelastic phenomena at small x . This has included a survey of the theoretical expectations for the small- x behavior of parton distributions as well as a summary of the available experimental data.

The small- x region is on the edge of applicability of perturbative QCD. Deeper (and further) understanding of physics at small x can come from the Regge theory and phenomenology, since the small- x limit of deep-inelastic scattering corresponds to the Regge limit. Out of many concepts of Regge theory that acquire a new content within perturbative QCD, the Pomeron certainly plays the most fundamental role. It determines, for example, the small- x behavior of the gluon and sea-quark distributions. Perturbative calculations predict that parton distributions rise very steeply in the small- x limit. This behavior must be slowed down (and finally tamed) in order to satisfy unitarity. This is achieved by including screening (shadowing) corrections in the evolution equations for the parton distributions. For $x \rightarrow 0$, the screen-

ing effect leads to saturation of the parton distributions with a linear dependence on Q^2 instead of a mild logarithmic one as in perturbative QCD.

A quantitative understanding of the relation between the Regge and perturbative QCD approaches is the main challenge in small- x physics. The following problems have to be solved in particular: (i) region of validity of the standard Altarelli-Parisi equation, (ii) importance of the resummation of large $\ln(1/x)$ terms, (iii) region of validity of the partonic picture or boundaries of the saturation region, (iv) scenarios of the approach to the saturation limit, e.g., the “hot spots” picture.

The measurements in the low- x region extend down to $x = 0.00002$ and Q^2 below and above 1 GeV^2 . The free-nucleon structure function F_2 does not display any significant x dependence down to $x \sim 0.003$, and the Q^2 dependence of this structure function is linear in $\ln(Q^2)$, which is the same as at higher four-momentum transfers. The structure function F_2 of nucleons bound in nuclei show a significant x dependence for $x < 0.1$, which is interpreted as a nuclear shadowing effect. Shadowing becomes more pronounced with increasing A of the nucleus and does not show any significant Q^2 dependence for fixed x intervals. Many models in which shadowing may be due to partonic interactions as well as the vector-meson component of the virtual photon are trying to describe these data.

A strong increase in the parton distributions at small x is perhaps the most spectacular and dramatic prediction of perturbative QCD. This increase leads to a corresponding increase of F_2 and F_L . Figures 48–50 summarize the predictions for the small- x region that will be probed at the HERA ep collider. It may be seen that, although one should in principle be able to reveal details of the possible theoretical QCD scenarios at small x , the region of x that will be accessible at HERA, $x > 10^{-5}$, may not be sensitive to the expected saturation effects (Gribov *et al.*, 1983; Levin, 1991).

Our discussion has been almost exclusively limited to deep-inelastic lepton-hadron scattering. Nevertheless the singular small- x behavior of parton distributions should also manifest itself in various semihard processes in hadron-hadron collisions like minijet production, the W , Z , or Higgs production, etc. The next generation of hadronic colliders, such as the SSC and the LHC, will be capable of probing the parton distributions in these processes at still smaller values of x , where the differences between various theoretical scenarios become significantly amplified. Nevertheless, deep-inelastic lepton-hadron scattering will still remain the most direct tool for probing the quark and antiquark distributions in the nucleon. In this respect the chance to study ep collisions with the LHC facility would offer a unique opportunity to study the very-small- x region ($x \ll 10^{-4}$).

Note added. After this paper was completed we became aware of three events related to small- x physics:

(1) Very recently the Second Workshop on HERA Physics provided more detailed predictions of the possi-

bilities for investigating the small- x region at HERA (materials from the Workshop are published in *Proceedings of the Workshop “Physics at HERA,”* DESY Hamburg, 1991, edited by W. Buchmüller and G. Ingelman).

(2) New, still preliminary NMC data on the nucleon structure function F_2 have been presented (E.M. Kabuss, invited talk at the *DESY-Zeuthen Workshop on Deep Inelastic Scattering*, Teupitz, 1992). These data differ at low x from what was presented at the Geneva Conference (Bird *et al.*, 1991).

(3) A new structure-function analysis incorporating the above-mentioned NMC data (A. D. Martin, W. J. Stirling, and R. G. Roberts, Durham University preprint DTP/92/16) has been completed. The results of this analysis differ significantly from those of Kwieciński *et al.* (1990) in the region relevant for HERA.

ACKNOWLEDGMENTS

We wish to express our gratitude to our collaborators, with whom the results reviewed in this paper were obtained. We are particularly indebted to H. Abramowicz, E. Levin, A. Levy, T. Sloan, and G. Wolf for a careful reading of the manuscript and detailed remarks. M.K. acknowledges the support of the Polish Government and Ministry of Education Research Programs CPBP 01.03, 01.06 and GMEN 133/90. J.K. acknowledges partial support of the Polish Committee for Scientific Research Grant No. 2 0198 91 01. K.Ch. and M.K. would like to thank the DESY Directorate for supporting their visits at DESY.

REFERENCES

- Abraham, K. J., H. Jung, G. A. Schuler, and J. F. de Troconiz, 1991, in *Proceedings of the Large Hadron Collider Workshop, Aachen*, edited by G. Jarlskog and D. Rein (Report No. CERN 90-10).
- Abramowicz, H., K. Charchuła, M. Krawczyk, and A. Levy, 1991a, *Mod. Phys. Lett. A* **6**, 1361.
- Abramowicz, H., K. Charchuła, M. Krawczyk, A. Levy, and U. Maor, 1991b, “Some topics in ep scattering at HERA. Part II: Parton distributions in a photon,” preprint DESY 91-057.
- Abramowicz, H., E. M. Levin, A. Levy, and U. Maor, 1991, *Phys. Lett. B* **269**, 465.
- Akhundov, A. A., D. Yu. Bardin, and N. M. Shumeiko, 1977, *Sov. J. Nucl. Phys.* **26**, 660.
- Akhundov, A. A., D. Yu. Bardin, and N. M. Shumeiko, 1986, *Sov. J. Nucl. Phys.* **44**, 998.
- Alekhin, S. I., *et al.* (HERA and COMPAS Groups), 1987, “Compilation of cross sections,” Report No. CERN-HERA 87-01.
- Allasia, D., *et al.* (NMC), 1990, *Phys. Lett. B* **249**, 366.
- Altarelli, G., 1982, *Phys. Rep.* **81**, 1.
- Altarelli, G., and G. Parisi, 1977, *Nucl. Phys. B* **126**, 298.
- Amaudruz, P., *et al.* (NMC, NA37), 1991a, *Phys. Rev. Lett.* **66**, 2712.
- Amaudruz, P., *et al.* (NMC), 1991b, *Z. Phys. C* **51**, 387.

- Amadruz, P., *et al.* (NMC), 1992a, Nucl. Phys. B **371**, 3.
- Amadruz, P., *et al.* (NMC), 1992b, Z. Phys. C **53**, 73.
- Arneodo, M., *et al.* (EMC, NA28), 1988, Phys. Lett. B **211**, 493.
- Arneodo, M., *et al.* (EMC, NA28), 1990, Nucl. Phys. B **333**, 1.
- Arnold, R. G., *et al.* (SLAC, E139), 1984, Phys. Rev. Lett. **52**, 727.
- Arvidson, A. A., H. Calen, S. Dahlgren, P. Grafstrom, L. Gustafsson, E. Hagberg, S. Kullander, R. Dobison, and E. Watson, 1986, Nucl. Instrum. Methods A **251**, 437.
- Arvidson, A., *et al.*, 1987, "Inelastic cross section for 280 GeV muons scattered at small angles off different target nuclei," Uppsala University preprint ISV-PH 2/87.
- Ashman, J., *et al.* (EMC, NA2), 1988, Phys. Lett. B **202**, 603.
- Aubert, J. J., *et al.* (EMC, NA2), 1981, Z. Phys. C **10**, 101.
- Aubert, J. J., *et al.* (EMC, NA9), 1983, Phys. Lett. B **123**, 275.
- Aubert, J. J., *et al.* (EMC, NA2), 1984, Z. Phys. C **22**, 341.
- Aubert, J. J., *et al.* (EMC, NA2), 1986, Nucl. Phys. B **272**, 158.
- Aubert, J. J., *et al.* (EMC, NA2), 1987, Nucl. Phys. B **293**, 740.
- Badełek, B., and J. Kwieciński, 1992, Nucl. Phys. B **370**, 278.
- Balitskij, Ya. Ya., and L. N. Lipatov, 1978, Yad. Fiz. **28**, 1597 [Sov. J. Nucl. Phys. **28**, 822 (1978)].
- Barbagli, G., and G. D'Agostini, 1988, in *Proceedings of the HERA Workshop*, edited by R. D. Peccei (DESY, Hamburg), Vol. 1, p. 135.
- Bardin, D. Yu., and N. M. Shumeiko, 1979, Sov. J. Nucl. Phys. **29**, 449.
- Bari, G., *et al.* (BCDMS), 1985, Phys. Lett. B **163**, 282.
- Bartels, J., 1979, Nucl. Phys. B **151**, 293.
- Bartels, J., 1980, Acta Phys. Pol. B **11**, 281.
- Bartels, J., 1991, Particle World **2**, 46.
- Bartels, J., J. Blümlein, and G. Schuler, 1990, in *Proceedings of the Topical Workshop on the Small-x Behavior of Deep Inelastic Scattering Structure Functions in QCD*, DESY, Hamburg, Nucl. Phys. B (Proc. Suppl.) **18C**, p. 147.
- Bartels, J., J. Blümlein, and G. Schuler, 1991, Z. Phys. C **50**, 91.
- Bartels, J., and G. Ingelman, 1990, Phys. Lett. B **235**, 175.
- Bauer, T. H., R. D. Spital, D. R. Yennie, and F. M. Pipkin, 1978, Rev. Mod. Phys. **50**, 261 and references therein; **51**, 407(E).
- Benvenuti, A. C., *et al.* (BCDMS), 1989, Phys. Lett. B **223**, 485.
- Berge, P., *et al.* (CDHSW), 1991, Z. Phys. C **49**, 187.
- Berger, E. L., J. C. Collins, D. E. Soper, and G. Sterman, 1987, Nucl. Phys. B **286**, 704.
- Bilchak, C. L., D. Schildknecht, and J. D. Stroughair, 1988, Phys. Lett. B **214**, 441.
- Bilchak, C. L., D. Schildknecht, and J. D. Stroughair, 1989, B **233**, 461.
- Bird, I. G., *et al.* (NMC), 1991, in *Proceedings of the Joint International Lepton-Photon Symposium and Europhysics Conference on High Energy Physics*, Geneva, edited by S. Hegarty, K. Potter, and E. Quercigh (World Scientific, Singapore), Vol. 1, p. 147.
- Blümlein, J., M. Klein, Th. Naumann, and T. Riemann, 1988, in *Proceedings of the HERA Workshop*, edited by R. D. Peccei (DESY, Hamburg), Vol. 1, p. 67.
- Bodek, A., *et al.* (SLAC-MIT, E87), 1979, Phys. Rev. D **20**, 1471.
- Bodek, A., *et al.* (SLAC-MIT, E87), 1983, Phys. Rev. Lett. **50**, 1431.
- Bodek, A., S. Dasu, and S. E. Rock, 1991, in *Proceedings of the Joint International Lepton-Photon Symposium and Europhysics Conference on High Energy Physics*, Geneva, edited by S. Hegarty, K. Potter, and E. Quercigh (World Scientific, Singapore), Vol. 1, p. 160.
- Bonino, R., *et al.* (UA8), 1988, Phys. Lett. B **211**, 239.
- Bourrely, C., J. Soffer, and T. T. Wu, 1984a, Nucl. Phys. B **247**, 15.
- Bourrely, C., J. Soffer, and T. T. Wu, 1984b, Phys. Rev. Lett. **54**, 757.
- Bourrely, C., J. Soffer, and T. T. Wu, 1988, Z. Phys. C **37**, 369.
- Brodsky, S. J., and H. J. Lu, 1990, Phys. Rev. Lett. **64**, 1342.
- Bronzan, J. B., and R. L. Sugar, 1978, Phys. Rev. D **17**, 585.
- Brüll, A., *et al.* (NMC), 1991, in *Proceedings of the XXVI Recontres de Moriond*, edited by J. Tran Than Van (Editions Frontières, Gif-sur-Yvette), in press.
- Caldwell, D. O., *et al.*, 1979, Phys. Rev. Lett. **42**, 553 and references therein.
- Cardy, J. L., 1974, Phys. Lett. B **53**, 355.
- Cardy, J. L., 1975, Nucl. Phys. B **93**, 525.
- Catani, S., F. Fiorani, and G. Marchesini, 1990a, Phys. Lett. B **234**, 339.
- Catani, S., F. Fiorani, and G. Marchesini, 1990b, Nucl. Phys. B **336**, 18.
- Charchuła, K., M. Krawczyk, H. Abramowicz, and A. Levy, 1990, "Some topics in *ep* scattering at HERA. Part I: Parton distributions in a nucleon," preprint DESY 90-019.
- Charchuła, K., and M. Krawczyk, 1990, "A note on Gluon Distribution at Small *x*," DESY preprint 90/122.
- Cheng, H., and T. T. Wu, 1969, Phys. Rev. Lett. **24**, 1456 and references therein.
- Ciafaloni, M., 1988, Nucl. Phys. B **296**, 49.
- Close, F. E., J. Qiu, and R. G. Roberts, 1989, Phys. Rev. D **40**, 2820.
- Collins, P. D. B., 1977, *An Introduction to Regge Theory and High-Energy Physics* (Cambridge University, Cambridge).
- Collins, J., and J. Kwieciński, 1989, Nucl. Phys. B **316**, 307.
- Collins, J., and J. Kwieciński, 1990, Nucl. Phys. B **335**, 89.
- Cooper-Sarkar, A. M., G. Ingelman, K. R. Long, R. G. Roberts, and D. H. Saxon, 1988, Z. Phys. C **39**, 281.
- Covalan, R. J., and E. Predazzi, 1991, in *Problems of Fundamental Modern Physics*, edited by R. Cherubini, P. Dalpiaz, and B. Minetti (World Scientific, Singapore), p. 85.
- Cudell, J. R., A. Donnachie, and P. V. Landshoff, 1989, Nucl. Phys. B **322**, 55.
- D'Agostini, G., and D. Monaldi, 1990, Z. Phys. C **48**, 467.
- Dasu, S., *et al.* (SLAC, E140), 1988a, Phys. Rev. Lett. **60**, 2591.
- Dasu, S., *et al.* (SLAC, E140), 1988b, Phys. Rev. Lett. **61**, 1061.
- Diemoz, M., F. Ferroni, E. Longo, and G. Martinelli, 1988, Z. Phys. C **39**, 21.
- Dokshitzer, Yu. L., D. I. Dyakonov, and S. I. Troyan, 1980, Phys. Rep. **58**, 265.
- Donnachie, A., and P. V. Landshoff, 1984, Nucl. Phys. B **244**, 322.
- Donnachie, A., and P. V. Landshoff, 1987, Phys. Lett. B **191**, 309.
- Donnachie, A., and P. V. Landshoff, 1989, Nucl. Phys. B **311**, 509.
- Eichten, E. J., C. Quigg, I. Hinchliffe, and K. D. Lane, 1984, Rev. Mod. Phys. **56**, 579; **58**, 1065(E).
- Feltesse, J., 1988, in *Proceedings of the HERA Workshop*, edited by R. D. Peccei (DESY, Hamburg), Vol. 1, p. 33.
- Feltesse, J., 1992, "HERA: The New frontier," preprint DAPNIA-SPP-91-01.
- Franco, V., and R. J. Glauber, 1966, Phys. Rev. **142**, 1195.
- Frankfurt, L. L., and M. I. Strikman, 1988, Phys. Rep. **160**, 235 and references therein.
- Frankfurt, L. L., and M. I. Strikman, 1989, Nucl. Phys. B **316**, 340.

- Franz, J., *et al.*, 1981, *Z. Phys. C* **10**, 105.
- Froissart, M., 1961, *Phys. Rev.* **123**, 1053.
- Frolov, G. V., V. N. Gribov, and L. N. Lipatov, 1970, *Phys. Lett. B* **31**, 34.
- Glück, M., R. M. Godbole, and E. Reya, 1988, "Parton distributions for high-energy colliders," University of Dortmund preprint DO-TH 88/18.
- Glück, M., R. M. Godbole, and E. Reya, 1989, *Z. Phys. C* **41**, 667.
- Glück, M., E. Reya, and A. Vogt, 1990, *Z. Phys. C* **48**, 471.
- Glück, M., E. Reya, and A. Vogt, 1991, *Z. Phys. C* **53**, 127.
- Gordon, B. A., *et al.* (CHIO), 1979, *Phys. Rev. D* **20**, 2645.
- Grammer, G., and J. D. Sullivan, 1978, in *Electromagnetic Interactions of Hadrons*, edited by A. Donnachie and G. Shaw (Plenum, New York), Vol. 2, p. 195.
- Gribov, L. V., E. M. Levin, and M. G. Ryskin, 1981a, *Nucl. Phys. B* **188**, 155.
- Gribov, L. V., E. M. Levin, and M. G. Ryskin, 1981b, *Sov. Phys. JETP* **53**, 1113.
- Gribov, L. V., E. M. Levin, and M. G. Ryskin, 1983, *Phys. Rep.* **100**, 1 and references therein.
- Gunion, J. F., and D. E. Soper, 1977, *Phys. Rev. D* **15**, 2677.
- Guy, J., *et al.* (BEBC), 1987, *Z. Phys. C* **36**, 337.
- Halliwell, C., *et al.* (FNAL, E665), 1991, in *Proceedings of the XXV International Conference on High Energy Physics*, edited by K. K. Phua and Y. Yamaguchi (World Scientific, Singapore), Vol. 1, p. 624.
- Halzen, F., and A. D. Martin, 1984, *Quarks and Leptons* (Wiley, New York).
- Harriman, P. N., A. D. Martin, R. G. Roberts, and W. J. Stirling, 1990, *Phys. Rev. D* **42**, 798.
- Ingelman, G., 1990, in *Proceedings of the Topical Workshop on the Small-x Behavior of Deep Inelastic Scattering Structure Functions in QCD*, DESY, Hamburg, *Nucl. Phys. B (Proc. Suppl.)* **18C**, p. 172.
- Ingelman, G., and E. Schlein, 1985, *Phys. Lett. B* **152**, 256.
- Jaffe, D. E., *et al.* (FNAL, E665), 1991, in *Proceedings of the XXVI Rencontres de Moriond*, edited by J. Tran Than Van (Editions Frontières, Gif-sur-Yvette), in press.
- Jarozewicz, T., 1980, *Acta Phys. Pol. B* **11**, 965.
- Jarozewicz, T., 1982, *Phys. Lett. B* **116**, 291.
- Krawczyk, M., 1990, in *Proceedings of the Topical Workshop on the Small-x Behaviour of Deep Inelastic Scattering Structure Functions in QCD*, DESY, Hamburg, *Nucl. Phys. B (Proc. Suppl.)* **18C**, p. 64.
- Kumano, S., and J. T. Londergan, 1990, "On the origin of isospin breaking in quark parton distributions," Indiana University preprint IU/NTC 90-16.
- Kuraev, E. A., L. N. Lipatov, and V. S. Fadin, 1977, *Zh. Eksp. Teor. Fiz.* **72**, 373 [*Sov. Phys. JETP* **45**, 199 (1977)].
- Kwieciński, J., 1985a, *Z. Phys. C* **29**, 561.
- Kwieciński, J., 1985b, *Z. Phys. C* **29**, 147.
- Kwieciński, J., 1990, *Z. Phys. C* **45**, 461.
- Kwieciński, J., and B. Badełek, 1988, *Phys. Lett. B* **208**, 508.
- Kwieciński, J., and B. Badełek, 1989, *Z. Phys. C* **43**, 251.
- Kwieciński, J., A. D. Martin, R. G. Roberts, and W. J. Stirling, 1990, *Phys. Rev. D* **42**, 3645.
- Kwieciński, J., A. D. Martin, and P. J. Sutton, 1991a, *Phys. Lett. B* **264**, 199.
- Kwieciński, J., A. D. Martin, and P. J. Sutton, 1991b, *Phys. Rev. D* **44**, 260.
- Landshoff, P. V., and O. Nachtmann, 1987, *Z. Phys. C* **35**, 405.
- Landshoff, P. V., and J. C. Polkinghorne, 1972, *Phys. Rep.* **5**, 1.
- Levin, E. M., 1991, "Orsay lectures on low x deep inelastic scattering," preprint LPTHE Orsay 91/02.
- Levin, E. M., and M. G. Ryskin, 1990a, *Phys. Rep.* **189**, 267.
- Levin, E. M., and M. G. Ryskin, 1990b, in *Proceedings of the Topical Workshop on the Small-x Behaviour of Deep Inelastic Scattering Structure Functions in QCD*, DESY, Hamburg [*Nucl. Phys. B (Proc. Suppl.)* **18C**, 92].
- Lietzke, C., and S. J. Wimpenny, 1989, "A Comparison of the RadEMC and Bardin-Shumeiko Radiative Correction Programs," University of California (Riverside) preprint UCR/DIS-89-06.
- Lipatov, L. N., 1976, *Yad. Fiz.* **23**, 642 [*Sov. J. Phys.* **23**, 338 (1976)].
- Lipatov, L. N., 1986, *Sov. Phys. JETP* **63**, 904 and references therein.
- Lipatov, L. N., 1989, in *Perturbative QCD*, edited by A. H. Mueller (World Scientific, Singapore), p. 411.
- Lipatov, L. N., and L. Szymanowski, 1980, "Some remarks on the Pomeron singularity in non-Abelian gauge theories," Warsaw Institute of Nuclear Studies, preprint IBJ No. 11/VII/80.
- Lohmann, W., and A. A. Akhundov, 1990, "The treatment of the radiative corrections in a deep inelastic muon scattering experiment," Institute of High Energy Physics (Zeuthen) preprint PHE-90-32.
- Low, S. E., 1975, *Phys. Rev. D* **12**, 163.
- Macfarlane, D. B., *et al.* (CCFR), 1984, *Z. Phys. C* **26**, 1.
- Marchesini, G., and B. R. Webber, 1990, in *Proceedings of the Topical Workshop on the Small-x Behaviour of Deep Inelastic Scattering Structure Functions in QCD*, DESY, Hamburg [*Nucl. Phys. B (Proc. Suppl.)* **18C**, 38].
- Marchesini, G., and B. R. Webber, 1991, *Nucl. Phys. B* **349**, 617.
- Martin, A., 1982, *Z. Phys. C* **15**, 185 and references therein.
- Martin, A. D., R. G. Roberts, and W. J. Stirling, 1990, *Phys. Lett. B* **252**, 653.
- Milsztajn, A., A. Staude, K. M. Teichert, M. Virchaux, and R. Voss, 1991, *Z. Phys. C* **49**, 527.
- Mishra, S., *et al.* (CCFR), 1991, in *Proceedings of the Joint Int. Lepton-Photon Symposium and Europhysics Conference on High Energy Physics, Geneva*, edited by S. Hegarty, K. Potter, and E. Quercigh (World Scientific, Singapore), Vol. 1, p. 135.
- Mo, L. W., and Y. S. Tsai, 1969, *Rev. Mod. Phys.* **41**, 205.
- Morfin, J., and Wu-Ki Tung, 1991, *Z. Phys. C* **52**, 13.
- Mueller, A. H., 1990a, *Nucl. Phys. B* **335**, 115.
- Mueller, A. H., 1990b, in *Proceedings of the Topical Workshop on the Small-x Behaviour of Deep Inelastic Scattering Structure Functions in QCD*, DESY, Hamburg [*Nucl. Phys. B (Proc. Suppl.)* **18C**, 125].
- Mueller, A. H., and J. Qiu, 1986, *Nucl. Phys. B* **268**, 427.
- Nikolaev, N. N., and V. I. Zakharov, 1975, *Phys. Lett.* **55B**, 397.
- Nikolaev, N. N., and B. G. Zakharov, 1991, *Z. Phys. C* **49**, 607.
- Nikolaev, N. N., and B. G. Zakharov, 1992, *Z. Phys. C* **53**, 331.
- Nussinov, S., 1976, *Phys. Rev. D* **14**, 246.
- Piller, G., K. Takayanagi, and W. Weise, 1989, "Shadowing effects in deep inelastic lepton-nucleus scattering," University of Regensburg preprint TPR-89-40.
- Poucher, J. S., *et al.* (SLAC, E49a), 1974, *Phys. Rev. Lett.* **32**, 118.
- Poucher, J. S., *et al.* (SLAC, E49a), 1973, "High-energy single arm inelastic *ep* and *ed* scattering at 6 degrees and 10 degrees," Report No. SLAC-PUB-1309.
- Qiu, J., 1987, *Nucl. Phys. B* **291**, 746.
- Reya, E., 1981, *Phys. Rep.* **69**, 195.
- Ryskin, M. G., 1988, *Sov. J. Nucl. Phys.* **47**, 230.

- Ryskin, H. G., 1990, *Sov. J. Nucl. Phys.* **52**, 529.
- Schellman, H., *et al.* (FNAL, E665), 1991, in *Proceedings of the Joint International Lepton-Photon Symposium and Europhysics Conference on High Energy Physics*, Geneva, edited by S. Hegarty, K. Potter, and E. Quercigh (World Scientific, Singapore), Vol. 1, p. 151.
- Shaevitz, M., 1992, unpublished talk given at the 1992 Rencontre de Moriond.
- Shaw, G., 1989, *Phys. Lett. B* **228**, 125.
- Sloan, T., G. Smadja, and R. Voss, 1988, *Phys. Rep.* **162**, 45.
- Stein, S., *et al.* (SLAC, E61), 1975, *Phys. Rev. D* **12**, 1884.
- Streng, K. H., 1988, in *Proceedings of the HERA Workshop*, edited by R. Peccei (DESY, Hamburg), Vol. 1, p. 365.
- Tkaczyk, S. M., W. J. Stirling, and D. H. Saxon, 1988, in *Proceedings of the HERA Workshop*, edited by R. D. Peccei (DESY, Hamburg), Vol. 1, p. 265.
- Tsai, Y. S., 1971, "Radiative corrections to electron scattering," Report No. SLAC-PUB-848.
- Tung, Wu-Ki, 1989, *Nucl. Phys. B* **315**, 378.
- Tung, Wu-Ki, 1990, in *Proceedings of the Topical Workshop on the Small- x Behaviour of Deep Inelastic Scattering Structure Functions on QCD*, DESY, Hamburg [*Nucl. Phys. B (Proc. Suppl.)* **18C**, 55].
- Tung, Wu-Ki, J. G. Morfin, H. Schellman, S. Kunori, A. Caldwell, and F. Olness, 1989, "Structure functions and parton distributions," preprint FERMILAB-Conf-89/26.
- Varvell, K., *et al.* (BEBC), 1987, *Z. Phys. C* **36**, 1.
- White, A. R., 1979, *Nucl. Phys. B* **159**, 77.
- Whitlow, L. W., 1990, Ph.D. Thesis, "Deep inelastic structure functions from electron scattering on hydrogen and iron at $0.6 \text{ GeV}^2 \leq Q^2 \leq 30 \text{ GeV}^2$," SLAC-Report-357.
- Whitlow, L. W., *et al.* (SLAC), 1990, *Phys. Lett. B* **250**, 193.
- Wolf, G., 1990, in *Proceedings of the Workshop on Hadron Structure Functions and Parton Distributions*, edited by D. F. Geesaman, J. Morfin, C. Sazama, and W. K. Tung (World Scientific, Singapore), p. 453.
- Zoller, V. R., 1992a, *Phys. Lett. B* **279**, 145.
- Zoller, V. R., 1992b, *Z. Phys. C* **54**, 425.